HHS Public Access

Author manuscript

J Med Chem. Author manuscript; available in PMC 2022 June 24.

Published in final edited form as:

J Med Chem. 2021 June 24; 64(12): 8474–8485. doi:10.1021/acs.jmedchem.1c00414.

A Druglike Small Molecule that Targets r(CCUG) Repeats in Myotonic Dystrophy Type 2 Facilitates Degradation by RNA Quality Control Pathways

Sarah Wagner-Griffin,
Department of Chemistry, The Scripps Research Institute, 130 Scripps Way, Jupiter, Florida 33458, United States

Masahito Abe,
Department of Chemistry, The Scripps Research Institute, 130 Scripps Way, Jupiter, Florida 33458, United States

Raphael I. Benhamou,
Department of Chemistry, The Scripps Research Institute, 130 Scripps Way, Jupiter, Florida 33458, United States

Alicia J. Angelbello,
Department of Chemistry, The Scripps Research Institute, 130 Scripps Way, Jupiter, Florida 33458, United States

Kamalakannan Vishnu,
Department of Chemistry, The Scripps Research Institute, 130 Scripps Way, Jupiter, Florida 33458, United States

Jonathan L. Chen,
Department of Chemistry, The Scripps Research Institute, 130 Scripps Way, Jupiter, Florida 33458, United States

Jessica L. Childs-Disney,
Department of Chemistry, The Scripps Research Institute, 130 Scripps Way, Jupiter, Florida 33458, United States

Matthew D. Disney

Corresponding Author: disney@scripps.edu.

The authors declare the following competing financial interest(s): M.D.D. is a founder of Expansion Therapeutics, and K.V. and A.J.A are current employees of Expansion Therapeutics.

SUPPORTING INFORMATION

The Supporting Information is available free of charge at https://pubs.acs.org/doi/10.1021/acs.jmedchem.1c00414.

• Approximate IC_{50}s for the disruption of the $r(CCUG)^{exp}$–MBNL1 complex (Table S1); Sequences of primers (Table S2); Results of a high-throughput screen (Figure S1); Structures of compounds **1**–**44** (Figure S2); WaterLOGSY NMR analysis of **3** (Figure S3); WaterLOGSY NMR analysis of **4** (Figure S4); WaterLOGSY NMR analysis of **5** (Figure S5); WaterLOGSY NMR analysis of **7** (Figure S6); Two-dimensional NOESY NMR analysis (Figure S7); One-dimensional NMR analysis of compounds (Figure S8); Cell viability of DM2 fibroblasts **t**reated with **3**, **4**, **5**, and **7** (Figure S9); Structures of compounds **45**–**82** (Figure S10); Cell viability of DM2 fibroblasts treated with lead-optimized compounds (Figure S11); Cellular activity of compounds **63**, **78**, and **79** (Figure S12); Compound **63** does not affect MAP4K4 alternative splicing (Figure S13); Compound **63** has no effect on CNBP levels or IR exon 11 splicing (Figure S14); synthetic schemes, compound characterization; HPLC traces; and NMR spectra (PDF)

• All DM2 hit compounds (SMILES + DATA) (CSV)

Department of Chemistry, The Scripps Research Institute, 130 Scripps Way, Jupiter, Florida 33458, United States

Abstract

Myotonic dystrophy type 2 (DM2) is one of >40 microsatellite disorders caused by RNA repeat expansions. The DM2 repeat expansion, r(CCUG)^{exp} (where “exp” denotes expanded repeating nucleotides), is harbored in intron 1 of the CCHC-type zinc finger nucleic acid binding protein (CNBP). The expanded RNA repeat causes disease by a gain-of-function mechanism, sequestering various RNA-binding proteins including the pre-mRNA splicing regulator MBNL1. Sequestration of MBNL1 results in its loss-of-function and concomitant deregulation of the alternative splicing of its native substrates. Notably, this r(CCUG)^{exp} causes retention of intron 1 in the mature CNBP mRNA. Herein, we report druglike small molecules that bind the structure adopted by r(CCUG)^{exp} and improve DM2-associated defects. These small molecules were optimized from screening hits from an RNA-focused small-molecule library to afford a compound that binds r(CCUG)^{exp} specifically and with nanomolar affinity, facilitates endogenous degradation of the aberrantly retained intron in which it is harbored, and rescues alternative splicing defects.

INTRODUCTION

RNA repeat expansions cause >40 microsatellite disorders, including Huntington’s disease [HD, r(CAG)^{exp}], C9orf72 amyotrophic lateral sclerosis/frontotemporal dementia [c9ALS/FTD, r(G_4C_2)^{exp}], and myotonic dystrophy types 1 and 2 [DM1, r(CUG)^{exp} and DM2, r(CCUG)^{exp}, respectively]. (1) Repeat expansions cause disease through various mechanisms dependent upon its location within a gene. For example, an RNA gain-of-function mechanism occurs when repeat sequesters functionally inactivate proteins that regulate alternative pre-mRNA splicing. (2) Repeat expansions can also contribute to disease via an aberrant translational mechanism that generates toxic proteins, named repeat-associated non-ATG translation. (3) Recently, it was discovered that GC-rich RNA repeat expansions located in introns, such as r(CCUG)^{exp}, r(CUG)^{exp}, and r(G_4C_2)^{exp}, cause retention of the intron in which they are harbored in mature mRNA species. (4)

The DM2 repeat expansion, r(CCUG)^{exp}, is harbored in intron 1 of CCHC-type zinc finger nucleic acid binding protein gene (CNBP). (5) This r(CCUG)^{exp} folds into a structure containing repeating 2 × 2 CU/UC internal loops (Figure 1A), (6) which bind and sequester muscleblind-like 1 (MBNL1), an important regulator of alternative pre-mRNA splicing, in nuclear foci. (7,8) Sequestration of MBNL1 by r(CCUG)^{exp} results in pre-mRNA splicing defects of MBNL1-regulated genes. For example, insulin receptor (*IR*) exon 11 is excluded too frequently in DM2 cells (Figure 1B). (9) r(CCUG)^{exp} can also cause dysfunction through intron retention, where CNBP itself is mis-spliced, and the r(CCUG)^{exp}-containing intron 1 is retained in mature mRNA species (Figure 1C). (4)

We have previously shown that intron retention is due to MBNL1 binding; knock-down of MBNL1 reduces intron retention, whereas forced expression of MBNL1 increases intron retenion. (10) Thus, small-molecule recognition of r(CCUG)^{exp} liberates MBNL1 and rescues deregulated splicing events and intron retention. In particular, we have shown that

kanamycin A derivatives that bind r(CCUG)^{exp} can specifically improve DM2-associated defects and reduce the levels of intron 1 containing r(CCUG)^{exp}. (10) In another example of an intron-retained RNA repeat [r(CUG)^{exp} in intron 3 of transcription factor 4 mRNA (*TCF*4) in Fuchs endothelial corneal dystrophy (FECD)], (11) small-molecule binding results in decay of the r(CUG)^{exp}-containing intron 3 through the RNA exosome. (12) Thus, small-molecule recognition of RNA repeat expansions in retained introns can allow for targeted RNA degradation through stimulation of RNA quality control mechanisms. In addition to interfacing of disease-causing RNAs with endogenous decay pathways, other methods for targeted RNA degradation rely on chimeric compounds comprising an RNA-binding ligand attached to a cleaving module. However, this strategy increases compound molecular weight and can affect various pharmacological and physicochemical properties such as membrane permeability and solubility. (13–17)

Although our previous studies targeting r(CCUG)^{exp} showed that small molecules can indeed interface the toxic RNA with endogenous degradation pathways, the aminoglycosides from which they are derived are not particularly druglike and provide little opportunity for optimization. (10,18) Herein, we studied a collection of RNA-focused, druglike small molecules to target r(CCUG)^{exp}. Medicinal chemistry optimization of screening hits afforded a druglike small molecule that binds r(CCUG)^{exp} with nanomolar affinity, specifically degrades r(CCUG)^{exp}-containing intron 1, and improves DM2-associated defects.

RESULTS & DISCUSSION

Studying an RNA-Focused Small-Molecule Compound Collection for Targeting r(CCUG)

To identify novel small molecules that bind r(CCUG)^{exp}, a druglike RNA-focused small-molecule library containing 3271 compounds was employed. (19) This library was previously designed to contain structurally diverse small molecules that have chemotypes that confer avidity toward RNA. (19) These chemotypes include benzimidazoles, indoles, thiazoles, and quinazolines. Furthermore, the compounds in this library are druglike as defined by satisfying Lipinksi's Rule of 5, (20) where Log *P* is < 5, molecular weight is < 500, the number of hydrogen bond donors is <5, and the number of hydrogen bond acceptors is <10 (Figure 2A). Historically, druglikeness has been defined by satisfying the Rule of 5; however, an increasing number of approved orally bioavailable drugs fall outside of these guidelines, and parameters such as molecular weight are increasing. (21,22) On average, the library also contains similar physicochemical properties to known drugs in DrugBank (Figure 2A). (19) Thus, this library can be used to identify druglike small molecules that bind to RNA structures.

To identify compounds that bind r(CCUG)^{exp}, a previously reported time-resolved fluorescence resonance energy transfer (TR-FRET) assay was used that measures disruption of a preformed r(CCUG)$_{12}$–MBNL1 complex by small molecules or other modalities. (23,24) The 3271 member library was screened at 200 μM, and 44 compounds disrupted complex formation by >60%, which corresponds to three standard deviations from the mean (or 3σ), affording a hit rate of 1.34% (Figure S1 and Table S1). Of the 44 hits, 38 contained a similar substituted N2-phenylquinazoline-2,4-diamine core, while the other hits contained

benzimidazoles and indazoles (Figure S2). Importantly, these 44 compounds are druglike as they have similar physicochemical properties to the rest of the library and to known drugs in DrugBank (Figure 2A). On average, the 44 hit compounds have a molecular weight of 327 ± 35 g/mol, a c Log *P* of 3.2 ± 0.9, TPSA of 76 ± 15 Å, and 2.5 ± 0.9 hydrogen bond donors. The *in vitro* potencies (IC_{50}s) of the 44 compounds were then measured in the TR-FRET assay, affording seven compounds (**1**–**7**) with IC_{50}s < 50 μM (highlighted in red in Figures 2B,C and Table S1). Interestingly, all seven of these compounds contained the substituted N2-phenylquinazoline-2,4-diamine core.

Analysis of Hit Compounds

The binding of **1**–**7** to an RNA containing a single 2 × 2 CU/UC was further studied by NMR spectroscopy. Compounds **1**, **2**, and **6** showed significant aggregation in NMR experiments and were excluded from further analysis. In contrast, waterLOGSY spectra showed that **3**, **4**, **5**, and **7** bound to the RNA, based on positive phase signals in the presence of RNA (Figures S3–S6). To confirm these interactions, one-dimensional (1D) NMR spectra of **3**, **4**, **5**, and **7** bound to the RNA containing one 2×2 CU/UC internal loop were analyzed. Aromatic protons of the unbound RNA were assigned via a two-dimensional (2D) nuclear over-Hauser effect spectroscopy (NOESY) spectrum (Figure S7). Significant shifts in resonances corresponding to H6 and H8 protons of the RNA were observed in the presence of these four compounds, indicating binding to the RNA (Figure S8).

After confirming binding to r(CCUG) repeats by NMR spectroscopy, the compounds were evaluated for their ability to improve the deregulation of the *IR* exon 11 alternative splicing in DM2 patient-derived fibroblasts. All four compounds were well tolerated in the patient-derived fibroblasts, as no significant toxicity was observed up to a 20 μM dose (Figure S9). As previously mentioned, *IR* exon 11 is frequently excluded in DM2 patient-derived fibroblasts as compared to wild-type cells. Interestingly, the most potent compound, **7**, rescued splicing by ~50% at 5 μM (Figure 2D).

Synthesis and *In Vitro* Analysis of Derivatives of 7

To improve the potency of **7**, a library of derivatives that replace the functional groups on the N2-phenylquinazoline-2,4-diamine core was synthesized and then evaluated for disrupting the $r(CCUG)_{12}$–MBNL1 complex *in vitro*. As an overview of medicinal chemistry effort, analogues were synthesized to explore the quinazoline core (**54**–**61**), the aniline moiety (**45**–**53**), and combinations thereof (**62**–**64**) (Figures 3A and S10). Synthetically, compounds were prepared starting from 2,4-dichloroquinazoline or 2,4-dichloropyrimidine analogue, followed by the addition of 3-aminopropan-1-ol in a 4-position selective manner. The aniline derivatives at the N2 position were then installed in a microwave-assisted reaction (Scheme 1, Supporting Information). Of the nine compounds in which N2–2,3-dihydrobenzo[*b*][1,4]dioxine was replaced with various aniline analogues, three compounds containing 2-methylbenzooxazole (**49**), 2-methylbenzothiazole (**50**), and 1-methyl-1*H*-indazole (**51**) substituents had IC_{50}s that were ~2–8 times lower than **7** (IC_{50} = 48.2 ± 0.07 μM) (Figures 3A, S11, and Table S1). Eight derivatives (**54**–**61**) with various substitution patterns of quinazolines and fused pyrimidines were then evaluated, and one compound containing

6-methylquinazoline (**58**) was identified with an IC_{50} of 12.7 ± 0.2 μM, about 4 times more potent than **7** (Figures 3A, S11, and Table S1).

To combine features of the derivates with improved IC_{50}s, three additional compounds were synthesized that contained 6-methylquinazoline and 2-methylbenzooxazole (**62**), 2-methylbenzothiazole (**63**), and 1-methyl-1*H*-indazole (**64**) (Figures 3A, S11, and Table S1). Compounds **62** and **63** had slightly lower IC_{50}s than corresponding analogues without a methyl substituent at the 6 position (**49** and **50**, respectively), and **63** was the most potent compound synthesized thus far with an IC_{50} of 2.2 ± 0.5 μM (Figures 3A, S11, and Table S1).

To explore further SAR around the benzothiazole moiety of **63**, 18 analogues with extensions built onto benzothiazole were synthesized (Schemes 2 and 3 and Figures 3A and S10). Six of these analogues were synthesized via Suzuki coupling using a bromobenzothiazole intermediate of **63** (Intermediate D, Scheme 2). Notably, an aromatic ring was added to derivatives **65**–**70** to potentially add π-stacking interactions with $r(CCUG)^{exp}$'s internal loops and thereby enhance binding interactions. The other 12 analogues were synthesized via thermal amine replacement toward the corresponding bromobenzothiazole derivative of **63** (Intermediate D, Scheme 3). This series of compounds was designed to add functional groups that could potentially interact with the RNA such as those with a positive charge (**71**, **74**, **79**, and **82**), additional hydrogen bond donors and acceptors (**71**, **72**, **74**–**82**), or those with aromatic rings to form π–π interactions (**75**, **76**, **77**, and **81**). Within these analogues, seven compounds (**71**, **72**, **73**, **74**, **78**, **79**, and **82**; Figure 3C) had IC_{50}s < 5 μM and were chosen for further investigation, along with **63** (Figure 3B). Interestingly, four compounds (**71**–**74**) have IC_{50}s < 500 nM, which represents a 100-fold improvement in *in vitro* potency compared to the starting compound, **7**.

Evaluation of the Cellular Activity of Compounds

The eight compounds with *in vitro* IC_{50}s < 5 μM were studied in DM2 patient-derived fibroblasts, both for their effects on cell viability and for rescue of *IR* exon 11 splicing. For the latter, we compared the percentage of exon 11 excluded upon compound treatment to untreated DM2 patient-derived fibroblasts and untreated WT fibroblasts, as measured by RT-PCR analysis. The percent rescue of a compound that restores the splicing pattern to that observed in WT cells is set to 100. Compounds **64**, **65**, **71**, **72**, **73**, **74**, and **82** displayed significant toxicity at 5 μM (Figure S11) and were not further evaluated. Of compounds with no toxicity at 5 μM (**63**, **78**, and **79**), **63** and **78** significantly improved *IR* splicing at 5 μM, while **63** also rescued splicing, by ~30%, at 1 μM (Figures 3D and S12). Compound **79** did not significantly rescue splicing at any concentration studied (Figures 3D and S12). Interestingly, this derivative (**79**) is structurally similar to **64**; however, the addition of the di-*N*-methylated functional group ablated its cellular activity, which could be due to reduced cellular uptake or changes to subcellar localization. At 1 μM dose, **63** rescues *IR* splicing more potently than **7** (33 ± 5 vs 12 ± 5; $p = 0.026$), and thus **63** is the most potent compound identified in these studies for improving DM2-associated splicing defects in cells.

The affinity and specificity of **63** for r(CCUG)^{exp} were measured by microscale thermophoresis (MST). Compound **63** binds to r(CCUG)$_{12}$ with a $K_{d,app}$ of 192 ± 20 nM, while no binding was observed to a base-paired RNA that does not contain internal loops (K_d > 20 μM) (Figure 3E,F).

As **63** selectively bound to r(CCUG)$_{12}$ over a base-paired control, its ability to improve other DM2-associated defects was assessed in DM2 patient-derived fibroblasts. Compound **63** (5 μM) reduced the number of r(CCUG)^{exp}–MBNL1 nuclear foci per cell from 7 ± 1 in untreated patient-derived fibroblasts to 5 ± 0.5 in treated cells, or an ~30% reduction, as determined by RNA fluorescence *in situ* hybridization (FISH) and MBNL1 immunofluorescence (Figure 4A,B). This decrease in the number of nuclear foci correlates with the improvement in *IR* receptor splicing observed at 5 μM (Figure 3D) as MBNL1 is no longer sequestered in foci and can resume its normal function. Importantly, **63** did not affect *MAP4K4* exon 22a splicing, a NOVA-dependent splicing event (Figure S13). (25)

As mentioned above, r(CCUG)^{exp} causes the aberrant retention of the intron in which it is harbored in the mature mRNA. We have previously shown that small molecules that bind r(CCUG)^{exp} can rescue defects in intron retention by facilitating removal of the retained intron, which is subsequently degraded. (10) Thus, we evaluated **63**'s ability to rescue r(CCUG)^{exp}-mediated intron retention. Indeed, **63** significantly reduced the abundance of CNBP intron 1 in DM2 patient-derived fibroblasts at doses of 5 and 1 μM (Figure 4C), as determined by RT-qPCR. Importantly, **63** did not affect the levels of CNBP mature mRNA (Figure 4D). The effects on intron 1 levels were also specific to mutant CNBP containing r(CCUG)^{exp}, as no effects were observed in wild-type fibroblasts (Figure S14). Furthermore, **63** did not affect *IR* exon 11 inclusion in wild-type fibroblasts (Figure S14). Thus, **63** specifically improved r(CCUG)^{exp}-mediated defects that are dysregulated in DM2 including nuclear foci, *IR* splicing, and intron retention.

Implications for Targeted Degradation of r(CCUG)^{exp}

Importantly, all of the bioactive compounds identified herein possess druglike properties. The optimized compound, **63**, has a low molecular weight (379.48 g/mol) and has a similar number of hydrogen bond donors (n = 3) to known drugs in DrugBank (n = 5). Furthermore, **63** possesses a favorable c Log *P* (3.75) and TPSA (83 Å) and satisfies the Rule of 5 criteria for druglikeness. Through medicinal chemistry optimization of screening hits, we identified compounds with >10-fold improvement in *in vitro* activity for disruption of an r(CCUG)$_{12}$–MBNL1 complex. The most bioactive compound from lead optimization showed ~5-fold improvement in its ability to improve DM2-associated splicing defects. Importantly, this lead-optimized compound (**63**) also rescued r(CCUG)^{exp}-containing intron 1 retention, resulting in degradation of the expanded repeat but not the mature transcript.

Endogenous decay of r(CCUG)^{exp} activated by a small molecule could occur in the nucleus or the cytoplasm. If the small molecule bound the mutant allele in the cytoplasm, any MBNL1 bound to the cytoplasmic repeat expansion would be liberated and would return to the nucleus. Since r(CCUG)^{exp}–MBNL1 foci are not observed in the cytoplasm in the absence of compound in our imaging studies (Figure 4A), such a mechanism is unlikely.

Alternatively, the small molecule could bind the repeat expansion in the nucleus, freeing MBNL1, increasing intron 1's accessibility to the splicing machinery, reducing nuclear foci, and rescuing splicing defects. The liberated intron would then be shuttled through endogenous degradation pathways. In such a mechanism, intron 1 levels would be reduced while levels of the mature CNBP transcript would be unchanged. Collectively, our data (Figures 3 and 4) suggest that the latter, rather than the former, is the primary mode of action for **63**.

Targeted degradation is an emerging field for affecting the biological function of disease-causing RNAs. Thus far, targeted RNA degradation can be achieved through: (i) direct cleavage of RNAs through conjugation of an RNA-binding module to bleomycin or derivatives of bleomycin; (13,26) (ii) recruitment of a ribonuclease through ribonuclease targeting chimeras (RIBOTACs), comprising an RNA-binding module and a compound that recruits RNaseL; (14,27) and (iii) small molecules that degrade repeat-containing introns, likely by increasing the accessibility of the disease-causing RNA to endogenous decay mechanisms. (10,12) As the former two approaches require chimeric compounds, the molecular weights of such modalities are larger and can negatively alter physicochemical properties. Targeted degradation through endogenous RNA decay mechanisms, however, can be accomplished with monomeric small molecules. Herein, we show that it is indeed possible to degrade r(CCUG)^{exp} with druglike monomeric small molecules. Targeted degradation of RNA repeat expansions with monomeric compounds can have broad applications as other repeat expansions, such as r(G_4C_2)^{exp} that causes c9ALS/FTD or r(CUG)^{exp} that causes FECD, which are both found in retained introns. (4,28) Furthermore, targeted degradation of RNA through RNA quality control mechanisms may be broadly applicable with monomeric, druglike small molecules that recognize RNA structures.

Conclusions

We identified novel compounds that bind r(CCUG)^{exp} and improve DM2-associated defects in patient-derived cells by high-throughput screening of a druglike RNA-focused small molecule library. Lead chemical optimization of small molecule binders afforded a compound with 20-fold improvement *in vitro* activity and 5-fold improvement in cellular activity. The lead-optimized small molecule selectively improves various DM2-associated defects including retention of r(CCUG)^{exp}-containing intron 1, which is decayed in cells upon treatment with the compound. The physicochemical properties of the compounds identified herein indicate that druglike monomeric small molecules can indeed selectively bind RNA structures. The ability to selectively degrade introns containing RNA repeat expansions with druglike small molecules will have broad implications in drug discovery efforts toward targeting RNAs.

EXPERIMENTAL SECTION

General Synthetic Procedures

Reagents and solvents were purchased from commercial sources and used without further purification. Microwave (MW)-assisted reactions were performed by an Initiator + (Biotage).

Compounds were purified: (i) by Isolera One flash chromatography system (Biotage) using prepacked C18 columns (spherical 20–35 μm, Agela Technologies) or prepacked silica gel columns (spherical 20–35 μm, Agela Technologies) or (ii) by high-performance liquid chromatography (HPLC) (Waters 2489 and 1525) using a SunFire Prep C18 OBD 5 μm column (19 mm × 150 mm) with a 5 mL/min flow. HPLC purity analysis was performed using a SunFire C18 3.5 μm column (4.6 mm × 150 mm) with a linear gradient (0–100% methanol (MeOH) + 0.1% (v/v) trifluoracetic acid (TFA) and water + 0.1% (v/v) TFA) over 60 min at a flow rate of 1 mL/min. The purity of all derivatives was evaluated via analytical HPLC and was >95% in all cases.

NMR spectra were collected on a 400 UltraShield (Bruker) (400 MHz for ^{1}H and 100 MHz for ^{13}C) or Ascend 600 (Bruker) (600 MHz for ^{1}H and 150 MHz for ^{13}C). Chemical shifts are reported in ppm relative to tetramethylsilane (TMS) for ^{1}H and residual solvent for ^{13}C as internal standards. Coupling constants (*J* values) are expressed in hertz.

High-resolution mass spectra were recorded on an Agilent 1260 Infinity LC system coupled to an Agilent 6230 TOF (HR-ESI) with a Poroshell 120 EC-C18 column (Agilent, 50 mm × 4.6 mm, 2.7 μm). Liquid chromatography–mass spectrometry (LCMS) analysis was performed by Agilent 1260 Infinity LC system coupled to an Agilent 6130 quadrupole LC/MS (ESI) with a ZORBAX SB-C18 column (Agilent, 50 mm × 2.1 mm, 1.8 μm). Compounds **1**–**44** were purchased from ChemBridge and used without further purification.

General Synthetic Procedure for 7, 45–64 (General Synthetic Procedure 1)

For **step 1**, a mixture of dichloroquinazoline (**A**) (0.469 mmol, 1.0 equiv) and 3-aminopropan-1-ol (1.52 mmol, 3.2 equiv) in isopropanol (IPA) (0.40 M) was heated at 85 °C for 30 min under MW irradiation. The reaction was cooled to room temperature, and product formation was confirmed by LCMS. The reaction mixture was then concentrated *in vacuo*, washed with H_2O (4 mL × 2), and dried to afford intermediate **B**. The material was used in the next reaction without further purification. Then in **step 2**, a mixture of **B** (79.5 μmol, 1.0 equiv) and a corresponding aniline (**C**) (159 μmol, 2.0 equiv) in ethanol (EtOH) was heated at 150 °C for 30–60 min under MW irradiation. The reaction was cooled to room temperature, and product formation was confirmed by LCMS. The reaction mixture was then concentrated *in vacuo* and purified by column chromatography [Agela Technologies, Silica, 20 g, 0–30% MeOH in dichloromethane (DCM)] to afford compounds **45**–**64**.

Synthesis of 7—Following general synthetic procedure 1 using 2,4-dichloroquinazoline (93.3 mg, 0.469 mmol) in **step 1** (obtained monochloro intermediate; 105.0 mg, 94%) and 2,3-dihydrobenzo[*b*][1,4]dioxin-6-amine (24.0 mg, 159 μmol) in **step 2** (18.9 mg, 79.5 μmol of monochloro intermediate) afforded 3-((2-((2,3-dihydrobenzo[*b*][1,4]dioxin-6-yl)amino)quinazolin-4-yl)amino)propan-1-ol (**7**) (12.2 mg, 44%). ^{1}H NMR (400 MHz, MeOD) δ 8.08 (d, *J* = 8.2 Hz, 1H), 7.78 (d, *J* = 7.4 Hz, 1H), 7.52 (d, *J* = 8.2 Hz, 1H), 7.45 (d, *J* = 7.4 Hz, 1H), 7.11–6.86 (m, 3H), 4.28 (s, 4H), 3.76 (t, *J* = 7.1 Hz, 2H), 3.67 (t, *J* = 6.1 Hz, 2H), and 2.00–1.90 (m, 2H). ^{13}C NMR (150 MHz, DMSO-d_6) δ 160.4, 154.7, 145.4, 143.5, 140.0, 134.2, 133.1, 123.9, 123.3, 121.7, 117.2, 114.4, 111.4, 110.1,

64.7, 64.4, 59.0, 38.9, and 32.1; HR-MS (ESI): calcd for $C_{19}H_{19}N_4O_3^-$ [M – H]$^-$; 351.1463; found, 351.1463.

Synthesis of 45—Following general synthetic procedure 1 using 2,4-dichloroquinazoline (93.3 mg, 0.469 mmol) in **step 1** (obtained monochloro intermediate; 105.0 mg, 94%) and benzo[*d*][1,3]dioxol-5-amine (21.8 mg, 159 μmol) in **step 2** (18.9 mg, 79.5 μmol of monochloro intermediate) afforded 3-((2-((4-methyl-3,4-dihydro-2*H*-benzo[*b*][1,4]oxazin-7-yl)amino)quinazolin-4-yl)amino)propan-1-ol (**45**) (16.6 mg, 62%). ^{1}H NMR (400 MHz, DMSO-d_6) δ 10.4 (br s, 1H), 9.89 (br s, 1H), 8.48–8.37 (m, 1H), 7.83–7.73 (m, 1H), 7.55–7.47 (m, 1H), 7.45–7.29 (m, 2H), 7.05–6.97 (m, 1H), 6.97–6.91 (m, 1H), 6.06 (s, 2H), 4.75–4.57 (m, 1H), 3.65–3.59 (m, 2H), 3.53–3.47 (m, 2H), and 1.87–1.78 (m, 2H); HR-MS (ESI): calcd for $C_{18}H_{17}N_4O_3^-$ [M – H]$^-$; 337.1306; found, 337.1321.

Synthesis of 46—Following general synthetic procedure 1 using 2,4-dichloroquinazoline (93.3 mg, 0.469 mmol) in **step 1** (obtained monochloro intermediate; 105.0 mg, 94%) and 2,2-difluorobenzo[*d*][1,3]dioxol-5-amine (27.5 mg, 159 μmol) in **step 2** (18.9 mg, 79.5 μmol of monochloro intermediate) afforded 3-((2-((2,2-difluorobenzo[*d*][1,3]dioxol-5-yl)amino)quinazolin-4-yl)amino)propan-1-ol (**46**) (12.4 mg, 42%). ^{1}H NMR (400 MHz, DMSO-d_6) δ 10.5 (br s, 1H), 9.77 (br s, 1H), 8.40–8.33 (m, 1H), 7.91–7.75 (m, 2H), 7.60–7.56 (m, 1H), 7.51–7.41 (m, 2H), 7.37–7.31 (m, 1H), 4.79–4.43 (m, 1H), 3.69–3.58 (m, 2H), 3.57–3.46 (m, 2H), and 1.87–1.78 (m, 2H); HR-MS (ESI): calcd for $C_{18}H_{15}F_2N_4O_3^-$ [M – H]$^-$; 373.1118; found, 373.1119.

Synthesis of 47—Following general synthetic procedure 1 using 2,4-dichloroquinazoline (93.3 mg, 0.469 mmol) in **step 1** (obtained monochloro intermediate; 105.0 mg, 94%) and 5-methyl-2,3-dihydrobenzo[*b*][1,4]dioxin-6-amine (26.3 mg, 159 μmol) in **step 2** (18.9 mg, 79.5 μmol of monochloro intermediate) afforded 3-((2-((5-methyl-2,3-dihydrobenzo[*b*][1,4]dioxin-6-yl)amino)quinazolin-4-yl)amino)propan-1-ol (**47**) (29.0 mg, 100%). ^{1}H NMR (400 MHz, DMSO-d_6) δ 9.86–8.69 (m, 2H), 8.24 (d, J = 7.8 Hz, 1H), 7.72–7.65 (m, 1H), 7.46 (d, J = 7.6 Hz, 1H), 7.35–7.27 (m, 1H), 6.96 (d, J = 8.6 Hz, 1H), 6.75 (d, J = 8.6 Hz, 1H), 4.58–4.54 (m, 1H), 4.33–4.28 (m, 2H), 4.27–4.22 (m, 2H), 3.59–3.49 (m, 2H), 3.49–3.43 (m, 2H), 2.06 (s, 3H), and 1.80–1.73 (m, 2H); HR-MS (ESI): calcd for $C_{20}H_{21}N_4O_3^-$ [M – H]$^-$; 365.1619; found, 365.1622.

Synthesis of 48—Following general synthetic procedure 1 using 2,4-dichloroquinazoline (93.3 mg, 0.469 mmol) in **step 1** (obtained monochloro intermediate; 105.0 mg, 94%) and 4-methyl-3,4-dihydro-2*H*-benzo[*b*][1,4]oxazin-7-amine (26.1 mg, 159 μmol) in **step 2** (18.9 mg, 79.5 μmol of monochloro intermediate) afforded 3-((2-((4-methyl-3,4-dihydro-2*H*-benzo[*b*][1,4]oxazin-7-yl)amino)quinazolin-4-yl)amino)propan-1-ol (**48**) (6.3 mg, 22%). ^{1}H NMR (400 MHz, MeOD) δ 7.86–7.82 (m, 1H), 7.86–7.82 (m, 1H), 7.57–7.52 (m, 1H), 7.39–7.35 (m, 1H), 7.20 (d, J = 2.4 Hz, 1H), 7.16–7.11 (m, 1H), 7.01 (dd, J = 8.6, 2.5 Hz, 1H), 6.70 (d, J = 8.7 Hz, 1H), 4.31–4.27 (m, 1H), 3.72–3.65 (m, 4H), 3.21–3.17 (m, 2H), 2.84 (s, 3H), and 1.97–1.88 (m, 2H); HR-MS (ESI): calcd for $C_{20}H_{22}N_5O_2^-$ [M – H]$^-$; 364.1779; found, 364.1786.

Synthesis of 49—Following general synthetic procedure 1 using 2,4-dichloroquinazoline (93.3 mg, 0.469 mmol) in **step 1** (obtained monochloro intermediate; 105.0 mg, 94%) and 2,3-dihydrobenzo[*b*][1,4]dioxin-6-amine (23.5 mg, 159 μmol) in **step 2** (18.9 mg, 79.5 μmol of monochloro intermediate) afforded 3-((2-((2-methylbenzo[*d*]oxazol-6-yl)amino)quinazolin-4-yl)amino)propan-1-ol (**49**) (8.2 mg, 30%). ^{1}H NMR (400 MHz, MeOD) δ 8.29 (d, *J* = 1.8 Hz, 1H), 7.94 (dd, *J* = 8.2, 1.0 Hz, 1H), 7.68–7.62 (m, 1H), 7.54–7.45 (m, 2H), 7.43 (dd, *J* = 8.6, 2.0 Hz, 1H), 7.29–7.23 (m, 1H), 3.75 (t, *J* = 7.0 Hz, 2H), 3.69 (t, *J* = 6.2 Hz, 2H), 2.63 (s, 3H), and 2.00–1.92 (m, 2H). ^{13}C NMR (150 MHz, DMSO-d_6) δ 163.1, 160.6, 151.2, 138.6, 135.8, 133.6, 128.5, 126.0, 124.3, 123.5, 122.7, 118.8, 117.0, 112.0, 101.6, 59.1, 38.7, 32.3, and 14.6; HR-MS (ESI): calcd for $C_{19}H_{18}N_5O_2^-$ [M – H]$^-$; 348.1466; found, 348.1470.

Synthesis of 50—Following general synthetic procedure 1 using 2,4-dichloroquinazoline (93.3 mg, 0.469 mmol) in **step 1** (obtained monochloro intermediate; 105.0 mg, 94%) and 2-methylbenzo[*d*]thiazol-6-amine (26.1 mg, 159 μmol) in **step 2** (18.9 mg, 79.5 μmol of monochloro intermediate) afforded 3-((2-((2-methylbenzo[*d*]thiazol-6-yl)amino)quinazolin-4-yl)amino)propan-1-ol (**50**) (7.7 mg, 27%). ^{1}H NMR (400 MHz, MeOD) δ 8.56 (d, *J* = 2.0 Hz, 1H), 7.93–7.88 (m, 1H), 7.70 (d, *J* = 8.8 Hz, 1H), 7.66–7.63 (m, 1H), 7.63–7.57 (m, 1H), 7.49–7.45 (m, 1H), 7.24–7.17 (m, 1H), 3.74 (t, *J* = 7.0 Hz, 2H), 3.70 (t, *J* = 6.2 Hz, 2H), 2.79 (s, 3H), and 2.00–1.92 (m, 2H). ^{13}C NMR (150 MHz, DMSO-d_6) δ 163.8, 160.6, 157.4, 151.4, 147.6, 139.5, 136.3, 133.0, 125.8, 123.2, 122.0, 121.9, 118.7, 112.2, 110.1, 59.2, 38.5, 32.4, and 20.1; HR-MS (ESI): calcd for $C_{19}H_{18}N_5OS^-$ [M – H]$^-$; 364.1238; found, 364.1245.

Synthesis of 51—Following general synthetic procedure 1 using 2,4-dichloroquinazoline (93.3 mg, 0.469 mmol) in **step 1** (obtained monochloro intermediate; 105.0 mg, 94%) and 1-methyl-1*H*-indazol-6-amine (23.4 mg, 159 μmol) in **step 2** (18.9 mg, 79.5 μmol of monochloro intermediate) afforded 3-((2-((1-methyl-1*H*-indazol-6-yl)amino)quinazolin-4-yl)amino)propan-1-ol (**51**) (25.4 mg, 92%). ^{1}H NMR (400 MHz, MeOD) δ 8.31 (br s, 1H), 7.97–7.93 (m, 1H), 7.89 (d, *J* = 0.9 Hz, 1H), 7.67–7.61 (m, 2H), 7.52–7.48 (m, 1H), 7.28–7.21 (m, 2H), 3.10 (s, 3H), 3.80 (t, *J* = 6.9 Hz, 2H), 3.69 (t, *J* = 6.1 Hz, 2H), and 2.02–1.94 (m, 2H); HR-MS (ESI): calcd for $C_{19}H_{19}N_6O^-$ [M – H]$^-$; 347.1626; found, 347.1630.

Synthesis of 52—Following general synthetic procedure 1 using 2,4-dichloroquinazoline (93.3 mg, 0.469 mmol) in **step 1** (obtained monochloro intermediate; 105.0 mg, 94%) and 1-methyl-1*H*-indazol-3-amine (23.4 mg, 159 μmol) in **step 2** (18.9 mg, 79.5 μmol of monochloro intermediate) afforded 3-((2-((1-methyl-1*H*-indazol-3-yl)amino)quinazolin-4-yl)amino)propan-1-ol (**52**) (5.2 mg, 19%). ^{1}H NMR (400 MHz, DMSO-d_6) δ 12.8 (br s, 0.5H), 11.5 (br s, 0.5H), 9.87 (br s, 1H), 8.51 (d, *J* = 8.1 Hz, 1H), 8.02 (d, *J* = 8.1 Hz, 1H), 7.90–7.82 (m, 1H), 7.79–7.72 (m, 1H), 7.68 (d, *J* = 8.6 Hz, 1H), 7.55–7.45 (m, 2H), 7.23–7.15 (m, 1H), 4.72–4.56 (m, 1H), 4.10 (3H, s), 3.75–3.56 (m, 2H), 3.52–3.39 (m, 2H), and 1.88–1.70 (m, 2H); HR-MS (ESI): calcd for $C_{19}H_{19}N_6O^-$ [M – H]$^-$; 347.1626; found, 347.1635.

Synthesis of 53—Following general synthetic procedure 1 using 2,4-dichloroquinazoline (93.3 mg, 0.469 mmol) in **step 1** (obtained monochloro intermediate; 105.0 mg, 94%) and *N*-methyl-2,3-dihydrobenzo[*b*][1,4]dioxin-6-amine (26.3 mg, 159 μmol) in **step 2** (18.9 mg, 79.5 μmol of monochloro intermediate) afforded 3-((2-((2,3-dihydrobenzo[*b*][1,4]dioxin-6-yl)(methyl)amino)quinazolin-4-yl)amino)propan-1-ol (**53**) (7.5 mg, 26%). ^{1}H NMR (400 MHz, DMSO-d_6) δ 9.63 (br s, 1H), 8.36 (d, J = 8.2 Hz, 1H), 7.75–7.69 (m, 2H), 7.40–7.34 (m, 1H), 7.04 (d, J = 2.2 Hz, 1H), 7.00–6.91 (m, 2H), 4.65–4.58 (m, 1H), 4.32–4.28 (m, 4H), 3.58–3.49 (m, 2H), 3.52 (s, 3H), 3.48–3.41 (m, 2H), and 1.81–1.70 (m, 2H); HR-MS (ESI): calcd for $C_{20}H_{21}N_4O_3^-$ [M – H]$^-$; 365.1619; found, 365.1636.

Synthesis of 54—Following general synthetic procedure 1 using 2,4-dichloro-5,6,7,8-tetrahydroquinazoline (95.2 mg, 0.469 mmol) in **step 1** (obtained monochloro intermediate; 86.3 mg, 76%) and 2,3-dihydrobenzo[*b*][1,4]dioxin-6-amine (24.0 mg, 159 μmol) in **step 2** (19.2 mg, 79.5 μmol of monochloro intermediate) afforded 3-((2-((2,3-dihydrobenzo[*b*][1,4]dioxin-6-yl)amino)-5,6,7,8-tetrahydroquinazolin-4-yl)amino)propan-1-ol (**54**) (15.4 mg, 54%). ^{1}H NMR (400 MHz, DMSO-d_6) δ 9.40 (br s, 1H), 7.60 (br s, 1H), 7.30 (d, J = 2.2 Hz, 1H), 7.01 (dd, J = 8.8, 2.2 Hz, 1H), 6.77 (d, J = 8.8 Hz, 1H), 4.54 (t, J = 4.7 Hz, 1H), 4.26–4.17 (m, 4H), 3.51–3.42 (m, 4H), 2.54–2.46 (m, 2H), 2.28–2.21 (m, 2H), and 1.79–1.66 (m, 6H); HR-MS (ESI): calcd for $C_{19}H_{23}N_4O_3^-$ [M – H]$^-$; 355.1778; found, 355.1773.

Synthesis of 55—Following general synthetic procedure 1 using 2,4-dichloro-5,7-dihydrofuro[3,4-*d*]pyrimidine (89.6 mg, 0.469 mmol) in **step 1** (obtained monochloro intermediate; 88.8 mg, 82%) and 2,3-dihydrobenzo[*b*][1,4]dioxin-6-amine (24.0 mg, 159 μmol) in **step 2** (18.2 mg, 79.5 μmol of monochloro intermediate) afforded 3-((2-((2,3-dihydrobenzo[*b*][1,4]dioxin-6-yl)amino)-5,7-dihydrofuro[3,4-*d*]pyrimidin-4-yl)amino)propan-1-ol (**55**) (7.8 mg, 29%). ^{1}H NMR (400 MHz, DMSO-d_6) δ 8.86 (br s, 1H), 7.45 (d, J = 2.5 Hz, 1H), 7.12 (dd, J = 8.8, 2.5 Hz, 1H), 7.02 (t, J = 5.2 Hz, 1H), 6.69 (d, J = 8.8 Hz, 1H), 4.80 (br s, 2H), 4.68–4.63 (m, 2H), 4.45 (t, J = 4.6 Hz, 1H), 4.23–4.13 (m, 4H), 3.53–3.38 (m, 4H), and 1.77–1.68 (m, 2H); HR-MS (ESI): calcd for $C_{17}H_{19}N_4O_4^-$ [M – H]$^-$; 343.1412; found, 343.1418.

Synthesis of 56—Following general synthetic procedure 1 using 4,6-dichloro-3-methyl-1*H*-pyrazolo[3,4-*d*]pyrimidine (95.2 mg, 0.469 mmol) in **step 1** (obtained monochloro intermediate; 44.0 mg, 39%) and 2,3-dihydrobenzo[*b*][1,4]dioxin-6-amine (24.0 mg, 159 μmol) in **step 2** (19.2 mg, 79.5 μmol of monochloro intermediate) afforded 3-((6-((2,3-dihydrobenzo[*b*][1,4]dioxin-6-yl)amino)-3-methyl-1*H*-pyrazolo[3,4-*d*]pyrimidin-4-yl)amino)propan-1-ol (**56**) (12.5 mg, 44%). ^{1}H NMR (400 MHz, DMSO-d_6) δ 12.4 (br s, 1H), 8.79 (br s, 1H), 7.62–7.41 (m, 1H), 7.20–7.05 (m, 1H), 6.91 (br s, 1H), 6.79–6.65 (m, 1H), 4.84–4.49 (m, 1H), 4.28–4.13 (m, 4H), 3.64–3.50 (m, 4H), 2.45 (br s, 3H), and 1.85–1.74 (m, 2H); HR-MS (ESI): calcd for $C_{17}H_{19}N_6O_3^-$ [M – H]$^-$; 355.1524; found, 355.1537.

Synthesis of 57—Following general synthetic procedure 1 using 2,4-dichloro-8-methylquinazoline (100.0 mg, 0.469 mmol) in **step 1** (obtained monochloro intermediate;

104.6 mg, 89%) and 2,3-dihydrobenzo[*b*][1,4]dioxin-6-amine (24.0 mg, 159 μmol) in **step 2** (20.0 mg, 79.5 μmol of monochloro intermediate) afforded 3-((2-((2,3-dihydrobenzo[*b*][1,4]dioxin-6-yl)amino)-8-methylquinazolin-4-yl)amino)propan-1-ol (**57**) (4.2 mg, 14%). ^{1}H NMR (400 MHz, MeOD) δ 7.95 (d, *J* = 7.9 Hz, 1H), 7.34 (d, *J* = 7.3 Hz, 1H), 7.39–7.35 (m, 1H), 7.29–7.24 (m, 1H), 6.99 (d, *J* = 8.7, 2.6 Hz, 1H), 6.89 (d, *J* = 8.7 Hz, 1H), 4.31–4.25 (m, 4H), 3.78–3.74 (m, 2H), 3.67 (t, *J* = 6.2 Hz, 2H), 2.51 (s, 3H), and 1.99–1.91 (m, 2H); HR-MS (ESI): calcd for $C_{20}H_{21}N_4O_3^-$ [M – H]$^-$; 365.1619; found, 365.1628.

Synthesis of 58—Following general synthetic procedure 1 using 2,4-dichloro-6-methylquinazoline (100.0 mg, 0.469 mmol) in **step 1** (obtained monochloro intermediate; 103.8 mg, 88%) and 2,3-dihydrobenzo[*b*][1,4]dioxin-6-amine (24.0 mg, 159 μmol) in **step 2** (20.0 mg, 79.5 μmol of monochloro intermediate) afforded 3-((2-((2,3-dihydrobenzo[*b*][1,4]dioxin-6-yl)amino)-6-methylquinazolin-4-yl)amino)propan-1-ol (**58**) (9.0 mg, 31%). ^{1}H NMR (400 MHz, MeOD) δ 7.90 (br s, 1H), 7.65–7.60 (m, 1H), 7.41 (d, *J* = 8.5 Hz, 1H), 7.06 (br s, 1H), 6.95–6.88 (m, 2H), 4.27 (s, 4H), 3.75 (t, *J* = 7.1 Hz, 2H), 3.67 (t, *J* = 6.2 Hz, 2H), 2.47 (s, 3H), 1.99–1.89 (m, 2H). ^{13}C NMR (150 MHz, DMSO-d_6) δ 160.2, 152.4, 143.7, 140.9, 138.7, 136.4, 134.1, 131.3, 123.8, 118.6, 117.5, 115.6, 111.3, 110.7, 64.7, 64.5, 58.8, 39.3, 31.9, and 21.2; HR-MS (ESI): calcd for $C_{20}H_{21}N_4O_3^-$ [M – H]$^-$; 365.1619; found, 365.1622.

Synthesis of 59—Following general synthetic procedure 1 using 2,4-dichloro-6-fluoroquinazoline (101.8 mg, 0.469 mmol) in **step 1** (obtained monochloro intermediate; 93.8 mg, 78%) and 2,3-dihydrobenzo[*b*][1,4]dioxin-6-amine (24.0 mg, 159 μmol) in **step 2** (20.3 mg, 79.5 μmol of monochloro intermediate) afforded 3-((2-((2,3-dihydrobenzo[*b*][1,4]dioxin-6-yl)amino)-6-fluoroquinazolin-4-yl)amino)propan-1-ol (**59**) (8.0 mg, 27%). ^{1}H NMR (400 MHz, DMSO-d_6) δ 9.59 (br s, 1H), 8.92 (br s, 1H), 8.19–8.08 (m, 1H), 7.65–7.56 (m, 1H), 7.56–7.48 (m, 1H), 7.42–7.28 (m, 1H), 7.16–7.05 (m, 1H), 6.82 (d, *J* = 8.7 Hz, 1H), 4.64–4.50 (m, 1H), 4.29–4.18 (m, 4H), 3.65–3.56 (m, 2H), 3.56–3.49 (m, 2H), and 1.87–1.78 (m, 2H); HR-MS (ESI): calcd for $C_{19}H_{18}FN_4O_3^-$ [M – H]$^-$; 369.1368; found, 369.1375.

Synthesis of 60—Following general synthetic procedure 1 using 2,4-dichloro-7-fluoroquinazoline (101.8 mg, 0.469 mmol) in **step 1** (obtained monochloro intermediate; 46.1 mg, 38%) and 2,3-dihydrobenzo[*b*][1,4]dioxin-6-amine (24.0 mg, 159 μmol) in **step 2** (20.3 mg, 79.5 μmol of monochloro intermediate) afforded 3-((2-((2,3-dihydrobenzo[*b*][1,4]dioxin-6-yl)amino)-7-fluoroquinazolin-4-yl)amino)propan-1-ol (**60**) (3.0 mg, 10%). ^{1}H NMR (400 MHz, MeOD) δ 8.21–8.12 (m, 1H), 7.31–7.19 (m, 2H), 7.11–7.00 (m, 1H), 6.98–6.87 (m, 2H), 4.28 (s, 4H), 3.75 (t, *J* = 7.1 Hz, 2H), 3.67 (t, *J* = 6.1 Hz, 2H), and 1.99–1.90 (m, 2H); HR-MS (ESI): calcd for $C_{19}H_{18}FN_4O_3^-$ [M – H]$^-$; 369.1368; found, 369.1383.

Synthesis of 61—Following general synthetic procedure 1 using 2,4-dichloro-8-fluoroquinazoline (101.8 mg, 0.469 mmol) in **step 1** (obtained monochloro intermediate; 76.5 mg, 64%) and 2,3-dihydrobenzo[*b*][1,4]dioxin-6-amine (24.0 mg, 159 μmol) in **step 2** (20.3 mg, 79.5 μmol of monochloro intermediate was used) afforded 3-((2-((2,3-

dihydrobenzo[*b*][1,4]dioxin-6-yl)amino)-8-fluoroquinazolin-4-yl)amino)propan-1-ol (**61**) (11.5 mg, 39%). ^{1}H NMR (400 MHz, DMSO-d_6) δ 9.21 (br s, 1H), 8.38 (br s, 1H), 7.91 (d, *J* = 8.2 Hz, 1H), 7.73–7.56 (m, 1H), 7.51–7.40 (m, 1H), 7.30–7.21 (m, 1H), 7.17–7.07 (m, 1H), 6.75 (d, *J* = 8.7 Hz, 1H), 4.64–4.47 (m, 1H), 4.30–4.15 (m, 4H), 3.66–3.48 (m, 4H), and 1.90–1.78 (m, 2H); HR-MS (ESI): calcd for $C_{19}H_{18}FN_4O_3^-$ [M – H]$^-$; 369.1368; found, 369.1383.

Synthesis of 62—Following general synthetic procedure 1 using 2,4-dichloro-6-methylquinazoline (100.0 mg, 0.469 mmol) in **step 1** (obtained monochloro intermediate; 103.8 mg, 88%) and 2-methylbenzo[*d*]oxazol-6-amine (23.5 mg, 159 μmol) in **step 2** (20.0 mg, 79.5 μmol of monochloro intermediate) afforded 3-((6-methyl-2-((2-methylbenzo[*d*]oxazol-6-yl)amino)quinazolin-4-yl)amino)propan-1-ol (**62**) (6.2 mg, 21%). ^{1}H NMR (400 MHz, MeOD) δ 8.11 (d, *J* = 1.8 Hz, 1H), 7.84 (br s, 1H), 7.60–7.55 (m, 2H), 7.44–7.38 (m, 2H), 3.75 (t, *J* = 7.0 Hz, 2H), 3.67 (t, *J* = 6.1 Hz, 2H), 2.64 (s, 3H), 2.46 (s, 3H), and 2.00–1.92 (m, 2H). ^{13}C NMR (150 MHz, DMSO-d_6) δ 163.8, 160.3, 154.1, 151.1, 136.9, 135.8, 133.2, 128.6, 126.0, 123.3, 121.5, 119.1, 117.9, 111.3, 102.9, 58.9, 39.0, 32.0, 21.3, and 14.6; HR-MS (ESI): calcd for $C_{20}H_{20}N_5O_2^-$ [M – H]$^-$; 362.1623; found, 362.1624.

Synthesis of 63—Following general synthetic procedure 1 using 2,4-dichloro-6-methylquinazoline (100.0 mg, 0.469 mmol) in **step 1** (obtained monochloro intermediate; 103.8 mg 88%) and 2-methylbenzo[*d*]thiazol-6-amine (26.1 mg, 159 μmol) in **step 2** (20.0 mg, 79.5 μmol of monochloro intermediate) afforded 3-((6-methyl-2-((2-methylbenzo[*d*]thiazol-6-yl)amino)quinazolin-4-yl)amino)propan-1-ol (**63**) (15.4 mg, 56%). ^{1}H NMR (400 MHz, MeOD) δ 8.31 (d, *J* = 2.0 Hz, 1H), 7.91–7.85 (m, 2H), 7.62–7.58 (m, 2H), 7.41 (d, *J* = 8.5 Hz, 1H), 3.76 (t, *J* = 7.1 Hz, 2H), 3.66 (t, *J* = 6.1 Hz, 2H), 2.83 (s, 3H), 2.47 (s, 3H), and 1.98–1.90 (m, 2H). ^{13}C NMR (150 MHz, DMSO-d_6) δ 164.7, 160.3, 155.4, 148.5, 145.9, 138.0, 136.2, 135.2, 132.2, 123.5, 122.8, 122.0, 119.6, 111.6, 59.1, 38.8, 32.3, 21.3, and 20.1; HR-MS (ESI): calcd for $C_{20}H_{22}N_5OS^-$ [M – H]$^-$; 378.1394; found, 378.1403.

Synthesis of 64—Following general synthetic procedure 1 using 2,4-dichloro-6-methylquinazoline (100.0 mg, 0.469 mmol) in **step 1** (obtained monochloro intermediate; 103.8 mg, 88%) and 1-methyl-1*H*-indazol-6-amine (23.4 mg, 159 μmol) in **step 2** (20.0 mg, 79.5 μmol of monochloro intermediate) afforded 3-((6-methyl-2-((1-methyl-1*H*-indazol-6-yl)amino)quinazolin-4-yl)amino)propan-1-ol (**64**) (7.9 mg, 27%). ^{1}H NMR (400 MHz, MeOD) δ 8.27 (br s, 1H), 7.89 (d, *J* = 0.9 Hz, 1H), 7.78 (br s, 1H), 7.67–7.63 (m, 1H), 7.53–7.48 (m, 1H), 7.41 (d, *J* = 8.5 Hz, 1H), 7.24–7.20 (m, 1H), 4.04 (s, 3H), 3.79 (t, *J* = 6.9 Hz, 2H), 3.69 (t, *J* = 6.1 Hz, 2H), 2.45 (s, 3H), and 2.02–1.93 (m, 2H); HR-MS (ESI): calcd for $C_{20}H_{21}N_6O^-$ [M – H]$^-$; 361.1782; found, 361.1778.

Synthesis of intermediate D—Following general synthetic procedure 1 using 2,4-dichloro-6-methylquinazoline (1.50 g, 7.04 mmol) in step 1 (obtained monochloro intermediate; 1.56 g, 88%) and 2-bromobenzo[*d*]thiazol-6-amine (500 mg, 2.18 mmol) in **step 2** (1.10 g, 4.37 mmol of monochloro intermediate) afforded 3-((2-((2-

bromobenzo[*d*]thiazol-6-yl)amino)-6-methylquinazolin-4-yl)amino)propan-1-ol (**D**) (1.00 g, quant). ^{1}H NMR (400 MHz, MeOD) δ 8.32–8.25 (m, 1H), 8.02–7.94 (m, 2H), 7.69 (dd, *J* = 8.5, 1.5 Hz, 1H), 7.64 (dd, *J* = 8.8, 2.2 Hz, 1H), 7.44 (d, *J* = 8.5 Hz, 1H), 3.80–3.74 (m, 2H), 3.65 (t, *J* = 6.1 Hz, 2H), 2.49 (s, 3H), and 1.99–1.89 (m, 2H); HR-MS (ESI): calcd for $C_{19}H_{18}BrN_5OS^+$ $[M + H]^+$; 444.0488; found, 444.04777.

General Synthetic Procedure for 65–70 (General Synthetic Procedure 2)

A mixture of 3-((2-((2-bromobenzo[*d*]thiazol-6-yl)amino)-6-methylquinazolin-4-yl)amino)propan-1-ol (**D**) (20.0 mg, 45.0 μmol, 1.0 equiv), Ar-boronic acid (67.5 μmol, 1.5 equiv), $Pd(PPh_3)_4$ (5.2 mg, 4.5 μmol, 0.1 equiv), and K_3PO_4 (19.1 mg, 90.0 μmol, 2.0 equiv) in dioxane/H_2O (2/1, 0.50 mL) was heated at 120 °C overnight. The reaction was cooled to room temperature, and product formation was confirmed by LCMS. The reaction mixture was then concentrated *in vacuo* and purified by column chromatography as described above (Agela Technologies, Silica, 20 g, 0–20% MeOH in DCM) and HPLC to afford compounds **65**–**70**.

Synthesis of 65—Following general synthetic procedure 2 using **D** (20.0 mg, 45.0 μmol) and (4-fluorophenyl)boronic acid (9.4 mg, 67.5 μmol) afforded 3-((2-((2-(4-fluorophenyl)benzo[*d*]thiazol-6-yl)amino)-6-methylquinazolin-4-yl)amino)propan-1-ol (**65**) (5.0 mg, 24%). ^{1}H NMR (400 MHz, DMSO-d_6) δ 12.6 (br s, 1H), 10.6 (br s, 1H), 9.55 (br s, 1H), 8.51 (br s, 1H), 8.19–8.06 (m, 4H), 7.73–7.65 (m, 2H), 7.54–7.40 (m, 3H), 4.79–4.49 (m, 1H), 3.72–3.63 (m, 2H), 3.57–3.49 (m, 2H), 2.43 (s, 3H), and 1.90–1.80 (m, 2H); HR-MS (ESI): calcd for $C_{25}H_{23}FN_5OS^+$ $[M + H]^+$; 460.1602; found, 460.1613.

Synthesis of 66—Following general synthetic procedure 2 using **D** (20.0 mg, 45.0 μmol) and (3-fluorophenyl)boronic acid (9.4 mg, 67.5 μmol) afforded 3-((2-((2-(3-fluorophenyl)benzo[*d*]thiazol-6-yl)amino)-6-methylquinazolin-4-yl)amino)propan-1-ol (**66**) (5.0 mg, 24%). ^{1}H NMR (400 MHz, DMSO-d_6) δ 12.7 (br s, 1H), 10.6 (br s, 1H), 9.58 (br s, 1H), 8.57 (br s, 1H), 8.15–8.07 (m, 2H), 7.96–7.87 (m, 2H), 7.75–7.61 (m, 3H), 7.53–7.42 (m, 2H), 4.77–4.56 (m, 1H), 3.72–3.63 (m, 2H), 3.57–3.49 (m, 2H), 2.43 (s, 3H), and 1.90–1.80 (m, 2H); HR-MS (ESI): calcd for $C_{25}H_{23}FN_5OS^+$ $[M + H]^+$; 460.1602; found, 460.1621.

Synthesis of 67—Following general synthetic procedure 2 using **D** (20.0 mg, 45.0 μmol) and *o*-tolylboronic acid (9.2 mg, 67.5 μmol) afforded 3-((6-methyl-2-((2-(*o*-tolyl)benzo[*d*]thiazol-6-yl)amino)quinazolin-4-yl)amino)propan-1-ol (**67**) (9.4 mg, 46%). ^{1}H NMR (400 MHz, DMSO-d_6) δ 12.6 (br s, 1H), 10.6 (br s, 1H), 9.60 (br s, 1H), 8.53 (br s, 1H), 8.16–8.07 (m, 2H), 7.83 (d, *J* = 7.3 Hz, 1H), 7.75–7.63 (m, 2H), 7.53–7.38 (m, 4H), 4.75–4.52 (m, 1H), 3.73–3.63 (m, 2H), 3.58–3.50 (m, 2H), 2.65 (s, 3H), 2.43 (s, 3H), and 1.91–1.80 (m, 2H); HR-MS (ESI): calcd for $C_{26}H_{26}N_5OS^+$ $[M + H]^+$; 456.1853; found, 456.1872.

Synthesis of 68—Following general synthetic procedure 2 using **D** (20.0 mg, 45.0 μmol) and (1H-pyrazol-3-yl)boronic acid (7.6 mg, 67.5 μmol) afforded 3-((2-((2-(1H-pyrazol-3-yl)benzo[*d*]thiazol-6-yl)amino)-6-methylquinazolin-4-yl)amino)propan-1-ol (**68**) (18.5 mg,

95%). ^{1}H NMR (400 MHz, DMSO-d_6) δ 13.4 (s, 1H), 12.5 (br s, 1H), 10.6 (br s, 1H), 9.66 (br s, 1H), 8.42 (br s, 1H), 8.19–7.93 (m, 3H), 7.71–7.60 (m, 2H), 7.54–7.46 (m, 1H), 6.93 (s, 1H), 4.73–4.57 (m, 1H), 3.72–3.62 (m, 2H), 3.57–3.49 (m, 2H), 2.43 (s, 3H), and 1.89–1.82 (m, 2H); HR-MS (ESI): calcd for $C_{22}H_{22}N_7OS^+$ [M + H]$^+$; 432.1601; found, 432.1613.

Synthesis of 69—Following general synthetic procedure 2 using **D** (20.0 mg, 45.0 μmol) and (4-carbamoylphenyl)boronic acid (11.1 mg, 67.5 μmol) afforded 4-(6-((4-((3-hydroxypropyl)amino)-6-methylquinazolin-2-yl)amino)benzo[*d*]thiazol-2-yl)benzamide (**69**) (12.5 mg, 57%). ^{1}H NMR (400 MHz, DMSO-d_6) δ 12.9 (br s, 1H), 10.7 (br s, 1H), 9.56 (br s, 1H), 8.59 (br s, 1H), 8.22–8.02 (m, 6H), 7.76–7.64 (m, 2H), 7.57 (s, 1H), 7.49 (d, J = 8.4 Hz, 1H), 6.93 (s, 1H), 4.78–4.52 (m, 1H), 3.76–3.62 (m, 2H), 3.60–3.51 (m, 2H), 2.43 (s, 3H), and 1.91–1.81 (m, 2H); HR-MS (ESI): calcd for $C_{26}H_{25}N_6O_2S^+$ [M + H]$^+$; 485.1754; found, 485.1778.

Synthesis of 70—Following general synthetic procedure 2 using **D** (20.0 mg, 45.0 μmol) and (1H-indol-5-yl)boronic acid (10.9 mg, 67.5 μmol) afforded 3-((2-((2-(1H-indol-5-yl)benzo[*d*]thiazol-6-yl)amino)-6-methylquinazolin-4-yl)amino)propan-1-ol (**70**) (19.6 mg, 91%). ^{1}H NMR (400 MHz, DMSO-d_6) δ 12.6 (br s, 1H), 11.5 (s, 1H), 10.6 (br s, 1H), 9.60 (br s, 1H), 8.43 (br s, 1H), 8.32 (d, J = 1.7 Hz, 1H), 8.13 (s, 1H), 8.03 (d, J = 8.7 Hz, 1H), 7.87 (dd, J = 8.5, 1.8 Hz, 1H), 7.71–7.61 (m, 2H), 7.59–7.48 (m, 3H), 6.64–6.61 (m, 1H), 4.83–4.44 (m, 1H), 3.72–3.63 (m, 2H), 3.57–3.51 (m, 2H), 2.43 (s, 3H), and 1.90–1.81 (m, 2H); HR-MS (ESI): calcd for $C_{27}H_{28}N_6OS^+$ [M + H]$^+$; 481.1805; found, 481.1829.

General Synthetic Procedure for 71–82 (General Synthetic Procedure 3)

A mixture of 3-((6-bromo-2-((2-methylbenzo[*d*]thiazol-6-yl)amino)quinazolin-4-yl)amino)propan-1-ol (**D**) (15.0 mg, 33.8 μmol, 1.0 equiv), *N,N*-diisopropylethylamine (DIPEA; 35.4 μL, 203 μmol, 6.0 equiv) and amine (203 μmol, 6.0 equiv) in 3-pentanol (0.10 M) was heated in a microwave vial at 120 °C overnight. The reaction was cooled to room temperature, and product formation was confirmed by LCMS. The reaction mixture was then concentrated *in vacuo* and purified by column chromatography (Biotage SNAP cartridge, KP-NH, 11g, 2%–30% MeOH in DCM) to afford compounds **71**–**82**.

Synthesis of 71—Following general synthetic procedure 3 using **D** (15.0 mg, 33.8 μmol) and 1-benzylpiperidin-4-amine (38.6 mg, 203 μmol) afforded 3-((2-((2-((1-benzylpiperidin-4-yl)amino)benzo[*d*]thiazol-6-yl)amino)-6-methylquinazolin-4-yl)amino)propan-1-ol (**71**) (13.8 mg, 74%). ^{1}H NMR (400 MHz, MeOD) δ 8.11 (d, J = 1.9 Hz, 1H), 7.71–7.67 (m, 1H), 7.46–7.25 (m, 9H), 3.81–3.64 (m, 5H), 3.56 (s, 2H), 2.97–2.86 (m, 2H), 2.42 (s, 3H), 2.28–2.19 (m, 2H), 2.13–2.04 (m, 2H), 1.96–1.89 (m, 2H), and 1.69–1.55 (m, 2H); HR-MS (ESI): calcd for $C_{31}H_{36}N_7OS^+$ [M + H]$^+$; 554.2697; found, 554.2722.

Synthesis of 72—Following general synthetic procedure 3 using **D** (15.0 mg, 33.8 μmol) and morpholine (17.7 mg, 203 μmol) afforded 3-((6-methyl-2-((2-morpholinobenzo[*d*]thiazol-6-yl)amino)quinazolin-4-yl)amino)propan-1-ol (**72**) (7.3 mg,

48%).^{1}H NMR (400 MHz, MeOD) δ 8.26 (d, *J* = 1.6 Hz, 1H), 7.71–7.67 (m, 1H), 7.48–7.40 (m, 3H), 7.33 (d, *J* = 8.5 Hz, 1H), 3.84–3.79 (m, 4H), 3.74–3.64 (m, 4H), 3.60–3.54 (m, 4H), 2.42 (s, 3H), and 2.00–1.89 (m, 2H). ^{13}C NMR (150 MHz, DMSO-d_6) δ 167.3, 160.2, 157.0, 149.7, 146.5, 136.9, 134.5, 131.0, 130.7, 125.6, 122.4, 118.9, 118.3, 111.9, 110.6, 66.0 (2C), 59.2, 48.7 (2C), 38.4, 32.4, and 21.3; HR-MS (ESI): calcd for $C_{23}H_{27}N_6O_2S^+$ [M + H]$^+$; 451.1911; found, 451.1929.

Synthesis of 73—Following general synthetic procedure 3 using **D** (15.0 mg, 33.8 μmol) and 2-methylpropan-1-amine (14.8 mg, 203 μmol) afforded 3-((2-((2-(isobutylamino)benzo[*d*]thiazol-6-yl)amino)-6-methylquinazolin-4-yl)amino)propan-1-ol (**73**) (11.6 mg, 79%). ^{1}H NMR (400 MHz, MeOD) δ 8.11 (d, *J* = 2.0 Hz, 1H), 7.70–7.67 (m, 1H), 7.45–7.38 (m, 2H), 7.35–7.31 (m, 2H), 3.74–3.65 (m, 4H), 3.23 (d, *J* = 7.0 Hz, 2H), 2.42 (s, 3H), 2.03–1.89 (m, 3H), 1.02 (s, 3H), and 1.00 (s, 3H). ^{13}C NMR (150 MHz, DMSO-d_6) δ 165.0, 160.2, 157.1, 149.8, 147.1, 136.2, 134.4, 130.7, 130.6, 125.6, 122.4, 117.9, 117.7, 111.8, 110.8, 59.3, 52.1, 38.4, 32.5, 28.2, 21.3, and 20.6 (2C); HR-MS (ESI): calcd for $C_{23}H_{27}N_6OS^-$ [M – H]$^-$; 435.1973; found, 435.1989.

Synthesis of 74—Following general synthetic procedure 3 using **D** (15.0 mg, 33.8 μmol) and 2-morpholinoethan-1-amine (26.4 mg, 203 μmol) afforded 3-((6-methyl-2-((2-((2-morpholinoethyl)amino)benzo[*d*]thiazol-6-yl)amino)quinazolin-4-yl)amino)propan-1-ol (**74**) (12.6 mg, 75%).^{1}H NMR (400 MHz, MeOD) δ 8.14–8.09 (m, 1H), 7.68 (br s, 1H), 7.45–7.29 (m, 4H), 3.77–3.63 (m, 8H), 3.57 (d, *J* = 6.4 Hz, 2H), 2.66 (d, *J* = 6.4 Hz, 2H), 2.60–2.49 (m, 4H), 2.41(s, 3H), and 1.98–1.88 (m, 2H). ^{13}C NMR (150 MHz, DMSO-d_6) δ 164.8, 160.2, 157.1, 149.8, 147.0, 136.3, 134.4, 130.8, 130.6, 125.6, 122.4, 118.0, 117.7, 111.9, 110.8, 66.6(2C), 59.3, 57.6, 53.8(2C), 41.5, 38.4, 32.5, 21.3; HR-MS (ESI): calcd for $C_{25}H_{32}N_7O_2S^+$ [M + H]$^+$; 494.2333; found, 494.2357.

Synthesis of 75—Following general synthetic procedure 3 using **D** (15.0 mg, 33.8 μmol) and benzo[*d*][1,3]dioxol-5-ylmethanamine (29.1 mg, 203 μmol) afforded 3-((2-((2-((benzo[*d*][1,3]dioxol-5-ylmethyl)amino)benzo[*d*]thiazol-6-yl)amino)-6-methylquinazolin-4-yl)amino)propan-1-ol (**75**) (8.9 mg, 51%). ^{1}H NMR (400 MHz, MeOD) δ 7.89 (s, 1H), 7.83 (d, *J* = 2.0 Hz, 1H), 7.60 (dd, *J* = 8.5, 1.4 Hz, 1H), 7.48 (d, *J* = 8.5 Hz, 1H), 7.40 (d, *J* = 8.5 Hz, 1H), 7.37–7.32 (m, 1H), 6.91–6.86 (m, 2H), 6.79 (d, *J* = 11.8 Hz, 1H), 5.93 (s, 2H), 4.54 (s, 2H), 3.74 (t, *J* = 7.1 Hz, 2H), 3.65 (t, *J* = 6.1 Hz, 2H), 2.46 (s, 3H), 1.98–1.88 (m, 2H); HR-MS (ESI): calcd for $C_{27}H_{27}N_6O_3S^+$ [M + H]$^+$; 515.1860; found, 515.1883.

Synthesis of 76—Following general synthetic procedure 3 using **D** (15.0 mg, 33.8 μmol) and 2-phenoxyethan-1-amine (27.8 mg, 203 μmol) afforded 3-((6-methyl-2-((2-((2-phenoxyethyl)amino)benzo[*d*]thiazol-6-yl)amino)quinazolin-4-yl)amino)propan-1-ol (**76**) (6.3 mg, 37%).^{1}H NMR (400 MHz, MeOD) δ 7.95–7.89 (m, 2H), 7.68–7.63 (m, 1H), 7.56–7.51 (m, 1H), 7.48–7.41 (m, 2H), 7.31–7.24 (m, 2H), 6.99–6.90 (m, 3H), 4.25 (t, *J* = 5.2 Hz, 2H), 3.90 (t, *J* = 5.2 Hz, 2H), 3.76 (t, *J* = 7.1 Hz, 2H), 3.65 (t, *J* = 6.1 Hz, 2H), 2.47 (s, 3H), and 1.98–1.88 (m, 2H); HR-MS (ESI): calcd for $C_{27}H_{27}N_6O_3S^+$ [M + H]$^+$; 515.1860; found, 515.1883.

Synthesis of 77—Following general synthetic procedure 3 using **D** (15.0 mg, 33.8 μmol) and 2-(benzyloxy)ethan-1-amine (30.7 mg, 203 μmol) afforded 3-((2-((2-((2-(benzyloxy)ethyl)amino)benzo[*d*]thiazol-6-yl)amino)-6-methylquinazolin-4-yl)amino)propan-1-ol (**77**) (7.7 mg, 44%). ^{1}H NMR (400 MHz, MeOD) δ 7.98–7.91 (m, 2H), 7.68–7.63 (m, 1H), 7.52–7.46 (m, 2H), 7.44 (d, *J* = 8.5 Hz, 1H), 7.36–7.21 (m, 5H), 4.59 (s, 2H), 3.79–3.70 (m, 6H), 3.65 (t, *J* = 6.1 Hz, 2H), 2.48 (s, 3H), and 1.98–1.88 (m, 2H); HR-MS (ESI): calcd for $C_{28}H_{31}N_6O_2S^+$ [M + H]$^+$; 515.2224; found, 515.2246.

Synthesis of 78—Following general synthetic procedure 3 using **D** (15.0 mg, 33.8 μmol) and 1-amino-2-methylpropan-2-ol (18.1 mg, 203 μmol) afforded 3-((2-((2-((2-hydroxy-2-methylpropyl)amino)benzo[*d*]thiazol-6-yl)amino)-6-methylquinazolin-4-yl)amino)propan-1-ol (**78**) (14.0 mg, 91%). ^{1}H NMR (400 MHz, MeOD) δ 8.12 (d, *J* = 2.1 Hz, 1H), 7.68 (br s, 1H), 7.44–7.37 (m, 2H), 7.35–7.30 (m, 2H), 3.73–3.64 (m, 4H), 3.44 (s, 2H), 2.41 (s, 3H), 1.98–1.87 (m, 2H), and 1.27 (s, 6H); HR-MS (ESI): calcd for $C_{23}H_{29}N_6O_2S^+$ [M + H]$^+$; 453.2067; found, 453.2069.

Synthesis of 79—Following general synthetic procedure 3 using **D** (15.0 mg, 33.8 μmol) and N1,N1-dimethylethane-1,2-diamine (17.9 mg, 203 μmol) afforded 3-((2-((2-((2-(dimethylamino)ethyl)amino)benzo[*d*]thiazol-6-yl)amino)-6-methylquinazolin-4-yl)amino)propan-1-ol (**79**) (12.9 mg, 84%). ^{1}H NMR (400 MHz, MeOD) δ 8.14 (d, *J* = 2.0 Hz, 1H), 7.68 (br s, 1H), 7.44–7.38 (m, 2H), 7.38–7.30 (m, 2H), 3.73–3.65 (m, 4H), 3.56 (t, *J* = 6.7 Hz, 2H), 2.64 (t, *J* = 6.7 Hz, 2H), 2.42 (s, 3H), 2.32 (s, 6H), and 1.98–1.89 (m, 2H); HR-MS (ESI): calcd for $C_{23}H_{30}N_7OS^+$ [M + H]$^+$; 452.2227; found, 452.2242.

Synthesis of 80—Following general synthetic procedure 3 using **D** (15.0 mg, 33.8 μmol) and 2,2′-azanediylbis(ethan-1-ol) (21.3 mg, 203 μmol) afforded 2,2′-((6-((4-((3-hydroxypropyl)amino)-6-methylquinazolin-2-yl)amino)benzo[*d*]thiazol-2-yl)azanediyl)bis(ethan-1-ol) (**80**) (5.2 mg, 33%). ^{1}H NMR (400 MHz, MeOD) δ 8.10–8.02 (m, 1H), 7.95–7.90 (m, 1H), 7.65 (dd, *J* = 8.5, 1.3 Hz, 1H), 7.56–7.50 (m, 2H), 7.44 (d, *J* = 8.5 Hz, 1H), 3.95–3.88 (m, 4H), 3.88–3.82 (m, 4H), 3.76 (t, *J* = 7.2 Hz, 2H), 3.66 (t, *J* = 6.1 Hz, 2H), 2.47 (s, 3H), and 1.98–1.88 (m, 2H); HR-MS (ESI): calcd for $C_{23}H_{29}N_6O_3S^+$ [M + H]$^+$; 469.2016; found, 469.2031.

Synthesis of 81—Following general synthetic procedure 3 using **D** (15.0 mg, 33.8 μmol) and 4-(2-aminoethyl)benzenesulfonamide (40.7 mg, 203 μmol) afforded 4-(2-((6-((4-((3-hydroxypropyl)amino)-6-methylquinazolin-2-yl)amino)benzo[*d*]thiazol-2-yl)amino)ethyl)benzenesulfonamide (**81**) (7.5 mg, 39%). ^{1}H NMR (400 MHz, MeOD) δ 7.94–7.91 (m, 1H), 7.91–7.82 (m, 3H), 7.67 (dd, *J* = 8.5, 1.4 Hz, 1H), 7.53–7.40 (m, 5H), 3.82–3.71 (m, 4H), 3.65 (t, *J* = 6.1 Hz, 2H), 3.11 (t, *J* = 7.0 Hz, 2H), 2.48 (s, 3H), and 1.99–1.89 (m, 2H); HR-MS (ESI): calcd for $C_{27}H_{30}N_7O_3S_2^+$ [M + H]$^+$; 564.1846; found, 564.1856.

Synthesis of 82—Following general synthetic procedure 3 using **D** (15.0 mg, 33.8 μmol) and 1-methylpiperazine (20.3 mg, 203 μmol) afforded 3-((6-methyl-2-((2-(4-methylpiperazin-1-yl)benzo[*d*]thiazol-6-yl)amino)quinazolin-4-yl)amino)propan-1-ol (**82**) (2.9 mg, 18%). ^{1}H NMR (400 MHz, MeOD) δ 8.25 (d, J = 1.7 Hz, 1H), 7.69 (br s, 1H), 7.47–7.39 (m, 3H), 7.37–7.30 (m, 1H), 3.75–3.58 (m, 8H), 2.65 (t, J = 10.2 Hz, 4H), 2.42 (s, 3H), 2.36 (s, 3H), and 1.98–1.88 (m, 2H); HR-MS (ESI): calcd for $C_{24}H_{30}N_7OS^+$ $[M + H]^+$; 464.2227; found, 464.2235.

High-Throughput Screen of the RNA-Focused Small-Molecule Library

Measurements for disruption of the r(CCUG)$_{12}$–MBNL1 complex were completed using a previously reported TR-FRET assay with minor modifications. (23,24) Briefly, 5′-biotinylated r(CCUG)$_{12}$ was folded in 1 × Folding Buffer (20 mM HEPES, pH 7.5, 110 mM KCl, and 10 mM NaCl) at 60 °C for 5 min then cooled to room temperature. The buffer was adjusted to 1 × Assay Buffer (20 mM HEPES, pH 7.5, 110 mM KCl, 10 mM NaCl, 2 mM $MgCl_2$, 2 mM $CaCl_2$, 5 mM DTT, 0.1% BSA, and 0.5% Tween-20). Then, MBNL1-His$_6$ was added, and the samples were incubated at room temperature for 15 min and added to a white 384-well plate using an Aurora FRD-IB reagent dispenser. Compounds from the RNA-focused small molecule library were then delivered to each well using a Beckman Biomek NXP liquid handler with a pin tool, and the samples were incubated for another 15 min at room temperature. The final concentration of r(CCUG)$_{12}$ was 80 nM, while the final concentration of MBNL1 was 60 nM. A solution of streptavidin-XL665 and anti-His$_6$-Tb antibody was then added to a total volume of 10 μL using an Aurora FRD-IB reagent dispenser, with final concentrations of 40 nM and 0.44 ng/μL, respectively. The sample plate was incubated for 30 min at room temperature and TR-FRET was measured on a Molecular Devices SpectraMax M5 plate reader using an excitation wavelength of 345 and a 420 nm cutoff. The ratios of fluorescence intensity at 545 and 665 nm were calculated, and ratios in the absence of a compound and in the absence of RNA were used to calculate percent disruption.

In Vitro IC_{50} Measurements

The IC_{50}s for disruption of r(CCUG)$_{12}$–MBNL1 by hit compounds from the RNA-focused small-molecule library were completed as described above except compounds were added manually to wells at varying concentrations to afford a dose response. The resulting curves were fit to eq 1 to determine IC_{50} values

$$y = B + \frac{A - B}{1 + \left(\frac{\mathrm{IC50}}{x}\right)^{\mathrm{hillslope}}} \quad (1)$$

where y is the ratio of fluorescence intensities at 545 and 665 nm (F545/F665), x is the concentration of a compound, B is F545/F665 value at max FRET effect (solution has RNA and protein but no compound added); A is F545/F665 value at min FRET effect (solution has antibodies but no RNA, protein, or compound); and IC_{50} is the concentration of a compound where half of the protein is displaced by a compound.

NMR Sample Preparation

A self-complementary RNA construct, r(5′-GACAGCCUGCUGUC-3′), was purchased from GE Healthcare Dharmacon, Inc., deprotected according to the manufacturer's recommended protocol, and desalted with PD-10 columns (GE Healthcare, cat: 17–0851-01) also per the manufacturer's protocol. RNA samples were dissolved in NMR Buffer [10 mM KH_2PO_4/K_2HPO_4 and 0.05 mM ethylenediamine tetraacetic acid (EDTA) (pH 6.0)] and folded by heating to 95 °C for 3 min and slowly cooling to room temperature.

NMR Spectroscopy

NMR spectra were acquired at 25 °C on Bruker Avance III 600 and 700 MHz spectrometers equipped with cryoprobes. One-dimensional NMR spectra were acquired on samples containing 100 μM of RNA alone in 100% D_2O. Compounds were each titrated into separate samples at 0.5, 1.0, 1.5, and 2.0 compound: RNA molar ratios. WaterLOGSY (water-ligand observed via gradient spectroscopy) spectra (29) were acquired on samples containing 300 μM of each compound alone or in the presence of 15 μM of RNA at a 20:1 compound: RNA ratio in H_2O, to which D_2O was added to 5% by volume. WaterLOGSY spectra were phased to give negative NOEs for nonbinders. Two-dimensional NOESY and DQF-COSY spectra were acquired on samples containing 400 μM of RNA alone in 100% D_2O. Two-dimensional NMR spectra were processed with nmrPipe (30) and assigned with SPARKY. (31)

Cell Lines and Cell Culture

Compounds were tested in two cell lines: (i) DM2 patient-derived fibroblasts (generous gift from University of Florida, Center for NeuroGenetics) and (ii) fibroblasts from a healthy donor (wild-type; WT GM07492; Coriell Institute). Cells were maintained at 37 °C with 5% CO_2. DM2 fibroblasts were cultured in Dulbecco's modified Eagle's medium (DMEM)/high glucose (HyClone) supplemented with 20% (v/v) fetal bovine serum (FBS) (Sigma) and 1% (v/v) antibiotic–antimycotic solution (Corning). Wild-type fibroblasts were cultured in MEM (Corning) supplemented with 10% (v/v) FBS, 1% (v/v) Glutagro (Corning), and 1% (v/v) antibiotic–antimycotic solution.

Evaluation of Cell Viability

Compound toxicity in DM2 fibroblasts was evaluated using a CellTiter-Glo Kit (Promega) as described in the manufacturer's protocol. Briefly, after 48 h treatment in 96-well plates, 100 μL of the CellTiter-Glo reagent was added to each well. The plate was then incubated at room temperature for 10 min, and luminescence was measured using BioTek FLX-800 luminescence plate reader (n = 6 replicates; 1 independent experiment).

Evaluation of Pre-mRNA Splicing via RT-PCR

Pre-mRNA splicing was analyzed as previously described. (10) Briefly, cells were grown in 6-well plates and treated with the desired compound in growth medium at ~40% confluency. After 48 h, the cells were lysed, and total RNA was harvested using a Zymo Quick RNA Miniprep Kit. Approximately 1 μg of total RNA was reverse transcribed using a qScript cDNA synthesis kit (20 μL of total reaction volume, Quanta BioSciences); 2 μL of the RT

reaction was used for PCR using GoTaq DNA polymerase (Promega). RT-PCR products were observed after 35 cycles of 95 °C for 30 s, 58 °C for 30 s, 72 °C for 1 min, and a final extension at 72 °C for 5 min. Products were separated on a 2% agarose gel (110 V for 1 h in 1 × TBE buffer), visualized by staining with ethidium bromide, and imaged using a Typhoon 9410 variable mode imager. Gels were quantified using ImageJ. Percent rescue was calculated by dividing the difference between treated and untreated DM2 samples by the difference between untreated DM2 and WT samples (eq 2).

$$\%\ \text{rescue} = \frac{\%\ \text{exon exclusion DM2} - \%\ \text{exon exclusion treated}}{\%\ \text{exon exclusion DM2} - \%\ \text{exon exclusion WT}} \times 100 \quad (2)$$

Evaluation of CNBP Abundance via RT-qPCR

CNBP abundance was evaluated as previously described. (10) Briefly, cells were grown in 6-well plates and treated with the desired compound in growth medium at 40% confluency. After 48 h, the cells were lysed, and total RNA was harvested using a Zymo Quick RNA Miniprep Kit per the manufacturer's protocol. Approximately 1 μg of total RNA was reverse transcribed using a qScript cDNA synthesis kit (20 μL of total reaction volume, Quanta BioSciences); 2 μL of the reverse transcription (RT) reaction was used for each primer pair (Table S2) for quantitative (q)PCR with SYBR Green Master Mix, performed on a QuantStudio 5, 384-well Block Real-Time PCR System (Applied Biosciences). Relative abundance was determined by normalizing to *GAPDH* (n = 6 replicates per concentration; 2 independent experiments).

Evaluation of Nuclear Foci via RNA Fluorescence *In Situ* Hybridization (FISH)

RNA FISH was used to determine the small molecules' effects on the number of nuclear foci as previously described. (10) The number of foci was counted in 40 nuclei/replicate (120 total nuclei counted); n = 3 replicates; 1 independent experiment.

Affinity Measurements

Binding affinity measurements were performed via microscale thermophoresis (MST) on a Monolith NT.115 system (NanoTemper Technologies) with Cy5-labeled $(CCUG)_{12}$ (5′-Cy5-GCG$(CCUG)_{12}$CGC; Dharmacon) and Cy5-labeled base pair control (BP; 5′-Cy5-GCG$(CCUG)_7(GCAG)_5$CGC; Dharmacon), which were deprotected according to the manufacturer's protocol and then desalted using a PD-10 column (GE LifeSciences) per the manufacturer's recommended procedure. RNA (5 nM) was prepared in 8 mM Na_2HPO_4, pH 7.0, 185 mM NaCl, and 1 mM EDTA and folded by heating at 60 °C for 5 min and slowly cooling to room temperature. Compound dilutions (1:1) were prepared using 1 × MST Buffer (8 mM Na_2HPO_4, pH 7.0, 185 mM NaCl, 1 mM EDTA) and 0.1% (v/v) Tween-20 was added. After cooling, the RNA solution was added to the compound solution (0.05% (v/v) Tween-20 final concentration). Samples were incubated for 30 min at room temperature and then loaded into standard capillaries (NanoTemper Technologies). The following parameters were used to acquire thermophoretic data: 5–20% LED, 80% MST power, laser-on time = 30 s, laser-off time = 5 s. Fluorescence was detected using excitation wavelengths of 605–645 nm and emission wavelengths of 680–685 nm. The resulting data

were analyzed by thermophoresis analysis and fitted using a quadratic binding equation in the MST analysis software (NanoTemper Technologies). Dissociation constants were then determined using eq 3. The reported K_d values are an average of two independent sets of experiments.

$$\text{fraction bound} = \frac{c + c_T + K_d - \sqrt{(c + C_T + K_d)^2 + 4cc_T}}{2c_T} \quad (3)$$

where c is the ligand concentration, c_T is the concentration of the RNA, and K_d is the dissociation constant.

SMILES and Physicochemical Properties

Marvin 20.8.0 (ChemAxon; https://www.chemaxon.com) was used to generate SMILES and to calculate physicochemical properties.

Supplementary Material

Refer to Web version on PubMed Central for supplementary material.

Acknowledgments

The authors thank the University of Florida, Center for NeuroGenetics for the generous gift of the DM2 fibroblast cell line used in this paper. The authors also thank the agencies that funded this work including the National Institutes of Health (R35 NS116846 to M.D.D. and F31-NS110269 to A.J.A., and S10-OD021550 to The Scripps Research Institute), the Muscular Dystrophy Association (grant 380467 to M.D.D.), the Myotonic US Fellowship Research grant (to R.I.B.), and to the National Ataxia Foundation Fellowship Research grant (to R.I.B.).

ABBREVIATIONS

CNBP	CCHC-type zinc finger nucleic acid binding protein
DCM	dichloromethane
DIPEA	*N,N*-diisopropylethylamine
DMF	dimethylformamide
DMSO	dimethyl sulfoxide
DM2	myotonic dystrophy type 2
HCl	hydrochloric acid
ESI	electrospray ionization
EtOH	ethanol
FISH	fluorescence *in situ* hybridization
HPLC	high-performance liquid chromatography
IPA	isopropanol

IR	insulin receptor
LCMS	liquid chromatography mass spectrometry
MBNL1	muscleblind-like 1
MeOH	methanol
MW	microwave
NMR	nuclear magnetic resonance
TFA	trifluoroacetic acid
TR-FRET	time-resolved fluorescence resonance energy transfer

REFERENCES

1. Paulson H Repeat expansion diseases. Handbook of Clinical Neurology; Elsevier, 2018; Vol. 147, pp 105–123. [PubMed: 29325606]
2. Hale MA; Johnson NE; Berglund JA Repeat-associated RNA structure and aberrant splicing. Biochim. Biophys. Acta, Gene Regul. Mech 2019, 1862, 194405, DOI: 10.1016/j.bbagrm.2019.07.006 [PubMed: 31323433]
3. Cleary JD; Pattamatta A; Ranum LPW Repeat-associated non-ATG (RAN) translation. J. Biol. Chem. 2018, 293, 16127–16141, DOI: 10.1074/jbc.R118.003237 [PubMed: 30213863]
4. Sznajder ŁJ; Thomas JD; Carrell EM; Reid T; McFarland KN; Cleary JD; Oliveira R; Nutter CA; Bhatt K; Sobczak K Intron retention induced by microsatellite expansions as a disease biomarker. Proc. Natl. Acad. Sci. U.S.A. 2018, 115, 4234, DOI: 10.1073/pnas.1716617115 [PubMed: 29610297]
5. Liquori CL; Ricker K; Moseley ML; Jacobsen JF; Kress W; Naylor SL; Day JW; Ranum LPW Myotonic dystrophy type 2 caused by a CCTG expansion in intron 1 of ZNF9. Science 2001, 293, 864, DOI: 10.1126/science.1062125 [PubMed: 11486088]
6. Childs-Disney JL; Yildirim I; Park H; Lohman JR; Guan L; Tran T; Sarkar P; Schatz GC; Disney MD Structure of the myotonic dystrophy type 2 RNA and designed small molecules that reduce toxicity. ACS Chem. Biol. 2014, 9, 538–550, DOI: 10.1021/cb4007387 [PubMed: 24341895]
7. Fardaei M; Rogers MT; Thorpe HM; Larkin K; Hamshere MG; Harper PS; Brook JD Three proteins, MBNL, MBLL and MBXL, co-localize in vivo with nuclear foci of expanded-repeat transcripts in DM1 and DM2 cells. Hum. Mol. Genet. 2002, 11, 805–814, DOI: 10.1093/hmg/11.7.805 [PubMed: 11929853]
8. Mankodi A; Urbinati CR; Yuan QP; Moxley RT; Sansone V; Krym M; Henderson D; Schalling M; Swanson MS; Thornton CA Muscleblind localizes to nuclear foci of aberrant RNA in myotonic dystrophy types 1 and 2. Hum. Mol. Genet. 2001, 10, 2165–2170, DOI: 10.1093/hmg/10.19.2165 [PubMed: 11590133]
9. Savkur RS; Philips AV; Cooper TA Aberrant regulation of insulin receptor alternative splicing is associated with insulin resistance in myotonic dystrophy. Nat. Genet. 2001, 29, 40–47, DOI: 10.1038/ng704 [PubMed: 11528389]
10. Benhamou RI; Angelbello AJ; Wang ET; Disney MD A toxic RNA catalyzes the cellular synthesis of its own inhibitor, shunting It to endogenous decay pathways. Cell Chem. Biol. 2020, 27, 223–231, DOI: 10.1016/j.chembiol.2020.01.003 [PubMed: 31981476]
11. Wieben ED; Aleff RA; Tosakulwong N; Butz ML; Highsmith WE; Edwards AO; Baratz KH A common trinucleotide repeat expansion within the transcription factor 4 (TCF4, E2–2) gene predicts Fuchs corneal dystrophy. PLoS One 2012, 7, e49083–e49086, DOI: 10.1371/journal.pone.0049083 [PubMed: 23185296]
12. Angelbello AJ; Benhamou RI; Rzuczek SG; Choudhary S; Tang Z; Chen JL; Roy M; Wang KW; Yildirim I; Jun AS A small molecule that binds an RNA repeat expansion stimulates its decay via

the exosome complex. Cell Chem. Biol. 2021, 28, 34–45, DOI: 10.1016/j.chembiol.2020.10.007 [PubMed: 33157036]

13. Angelbello AJ; Rzuczek SG; Mckee KK; Chen JL; Olafson H; Cameron MD; Moss WN; Wang ET; Disney MD Precise small-molecule cleavage of an r(CUG) repeat expansion in a myotonic dystrophy mouse model. Proc. Natl. Acad. Sci. U.S.A. 2019, 116, 7799–7804, DOI: 10.1073/pnas.1901484116 [PubMed: 30926669]
14. Costales MG; Aikawa H; Li Y; Childs-Disney JL; Abegg D; Hoch DG; Pradeep Velagapudi S; Nakai Y; Khan T; Wang KW Small-molecule targeted recruitment of a nuclease to cleave an oncogenic RNA in a mouse model of metastatic cancer. Proc. Natl. Acad. Sci. U.S.A. 2020, 117, 2406–2411, DOI: 10.1073/pnas.1914286117 [PubMed: 31964809]
15. Disney MD Targeting RNA with small molecules to capture opportunities at the intersection of chemistry, biology, and medicine. J. Am. Chem. Soc. 2019, 141, 6776–6790, DOI: 10.1021/jacs.8b13419 [PubMed: 30896935]
16. Benhamou RI; Angelbello AJ; Andrews RJ; Wang ET; Moss WN; Disney MD Structure-specific cleavage of an RNA repeat expansion with a dimeric small molecule is advantageous over sequence-specific recognition by an oligonucleotide. ACS Chem. Biol. 2020, 15, 485–493, DOI: 10.1021/acschembio.9b00958 [PubMed: 31927948]
17. Benhamou RI; Abe M; Choudhary S; Meyer SM; Angelbello AJ; Disney MD Optimization of the linker domain in a dimeric compound that degrades an r(CUG) repeat expansion in cells. J. Med. Chem. 2020, 63, 7827–7839, DOI: 10.1021/acs.jmedchem.0c00558 [PubMed: 32657583]
18. Wong C-H; Fu Y; Ramisetty SR; Baranger AM; Zimmerman SC Selective inhibition of MBNL1–CCUG interaction by small molecules toward potential therapeutic agents for myotonic dystrophy type 2 (DM2). Nucleic Acids Res. 2011, 39, 8881–8890, DOI: 10.1093/nar/gkr415 [PubMed: 21768123]
19. Haniff HS; Graves A; Disney MD Selective small molecule recognition of RNA base
20. Lipinski CA; Lombardo F; Dominy BW; Feeney PJ Experimental and computational approaches to estimate solubility and permeability in drug discovery and development settings. Adv. Drug Delivery Rev. 1997, 23, 3–25, DOI: 10.1016/S0169-409X(96)00423-1
21. Shultz MD Two decades under the influence of the Rule of Five and the changing properties of approved oral drugs. J. Med. Chem. 2019, 62, 1701–1714, DOI: 10.1021/acs.jmedchem.8b00686 [PubMed: 30212196]
22. DeGoey DA; Chen H-J; Cox PB; Wendt MD Beyond the Rule of 5: lessons learned from AbbVie's drugs and compound collection. J. Med. Chem. 2018, 61, 2636–2651, DOI: 10.1021/acs.jmedchem.7b00717 [PubMed: 28926247]
23. Costales MG; Rzuczek SG; Disney MD Comparison of small molecules and oligonucleotides that target a toxic, non-coding RNA. Bioorg. Med. Chem. Lett. 2016, 26, 2605–2609, DOI: 10.1016/j.bmcl.2016.04.025 [PubMed: 27117425]
24. Chen CZ; Sobczak K; Hoskins J; Southall N; Marugan JJ; Zheng W; Thornton CA; Austin CP Two high-throughput screening assays for aberrant RNA-protein interactions in myotonic dystrophy type 1. Anal. Bioanal. Chem. 2012, 402, 1889–1898, DOI: 10.1007/s00216-011-5604-0 [PubMed: 22218462]
25. Ule J; Ule A; Spencer J; Williams A; Hu JS; Cline M; Wang H; Clark T; Fraser C; Ruggiu M Nova regulates brain-specific splicing to shape the synapse. Nat. Genet. 2005, 37, 844–852, DOI: 10.1038/ng1610 [PubMed: 16041372]
26. Angelbello AJ; DeFeo ME; Glinkerman CM; Boger DL; Disney MD Precise targeted cleavage of a r(CUG) repeat expansion in cells by using a small-molecule–deglycobleomycin conjugate. ACS Chem. Biol. 2020, 15, 849–855, DOI: 10.1021/acschembio.0c00036 [PubMed: 32186845]
27. Haniff HS; Tong Y; Liu X; Chen JL; Suresh BM; Andrews RJ; Peterson JM; O'Leary CA; Benhamou RI; Moss WN Targeting the SARS-CoV-2 RNA genome with small molecule binders and ribonuclease targeting chimera (RIBOTAC) degraders. ACS Cent. Sci 2020, 6, 1713–1721, DOI: 10.1021/acscentsci.0c00984 [PubMed: 33140033]
28. DeJesus-Hernandez M; Mackenzie IR; Boeve BF; Boxer AL; Baker M; Rutherford NJ; Nicholson AM; Finch NA; Flynn H; Adamson J Expanded GGGGCC hexanucleotide repeat in noncoding

region of C9ORF72 causes chromosome 9p-linked FTD and ALS. Neuron 2011, 72, 245–256, DOI: 10.1016/j.neuron.2011.09.011 [PubMed: 21944778]

29. Dalvit C; Pevarello P; Tato M; Veronesi M; Vulpetti A; Sundstrom M Identification of compounds with binding affinity to proteins via magnetization transfer from bulk water. J. Biomol. NMR 2000, 18, 65–68, DOI: 10.1023/A:1008354229396 [PubMed: 11061229]
30. Delaglio F; Grzesiek S; Vuister GW; Zhu G; Pfeifer J; Bax A NMRPipe: A multidimensional spectral processing system based on UNIX pipes. J. Biomol. NMR 1995, 6, 277–293, DOI: 10.1007/BF00197809 [PubMed: 8520220]
31. Goddard TD; Kneller DG SPARKY, NMR Assignment and Integration Software, 3; University of California: San Francisco, 2004.

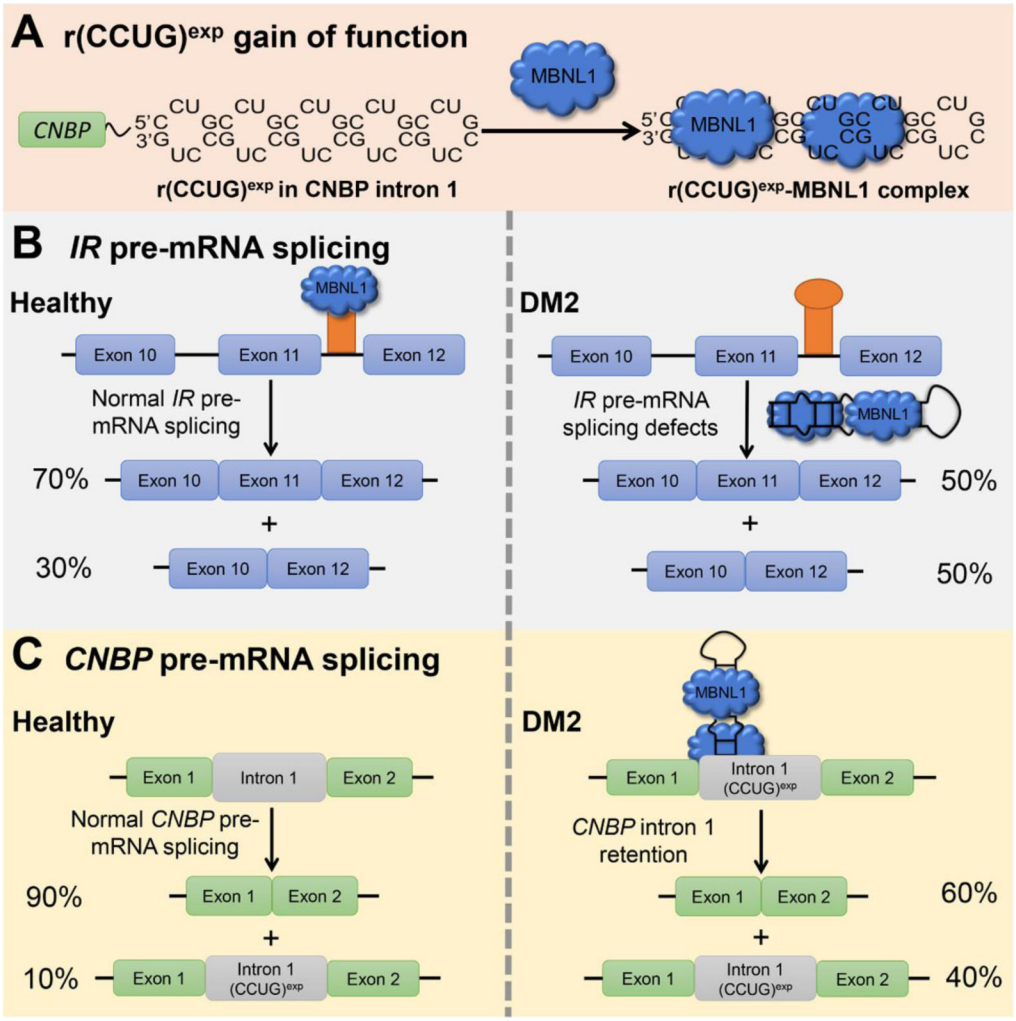

Figure 1.

r(CCUG)^{exp}-mediated defects in DM2. (A) DM2 is caused by r(CCUG)^{exp} in CNBP intron 1, which folds into a structure with repeating 2 × 2 nucleotide internal loops that sequester regulatory proteins involved in pre-mRNA splicing such as MBNL1. (B) Sequestration of MBNL1 by r(CCUG)^{exp} results in splicing defects in its native pre-mRNAs substrates. For example, *IR* exon 11 is included ~70% of the time in healthy cells, but only ~50% in DM2-affected cells. (C) r(CCUG)^{exp} also causes intron retention where intron 1 is aberrantly retained in CNBP mature RNA.

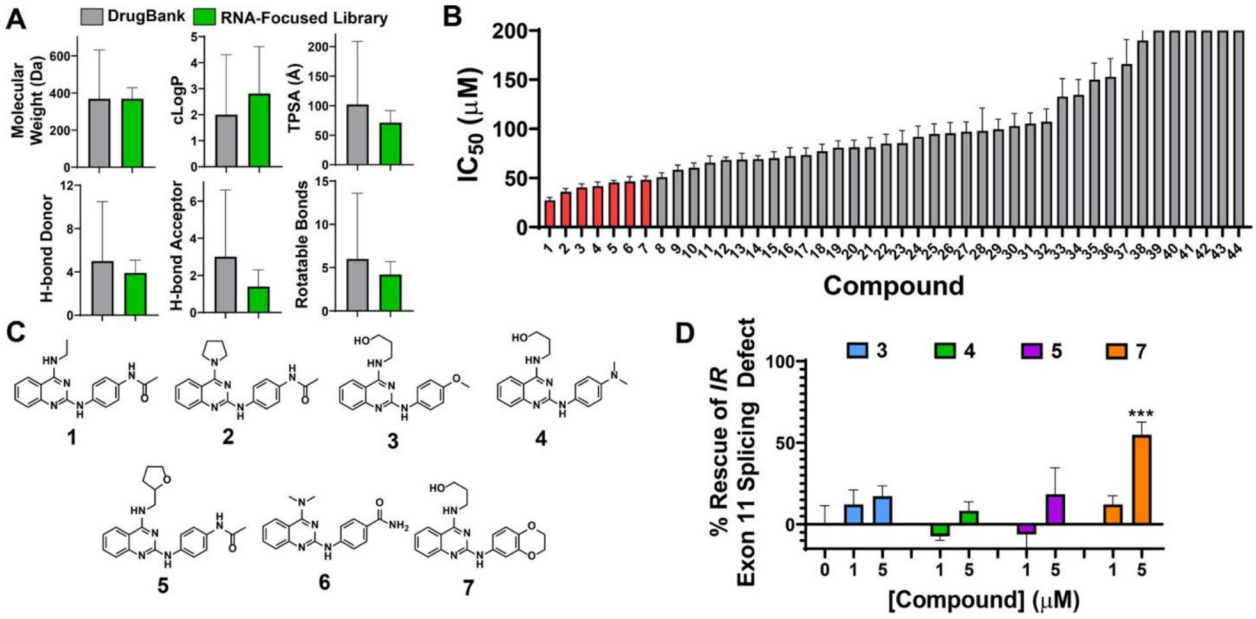

Figure 2.

Small molecules that inhibit r(CCUG)^{exp}–MBNL1 complex formation *in vitro*. (A) Characteristics of an RNA-focused small molecule library compared to characteristics of known drugs in DrugBank. (B) IC_{50} values of hit compounds from the RNA-focused library screen for disrupting the r(CCUG)$_{12}$–MBNL1 complex ($n = 2$). Molecules in red have IC_{50}s < 50 μM. (C) Chemical structures of compounds with IC_{50}s < 50 μM. (D) Rescue of the *IR* exon 11 splicing defect by **3**, **4**, **5**, and **7** in DM2 patient-derived fibroblasts ($n = 2$). Error bars represent standard deviation (SD) for all panels.

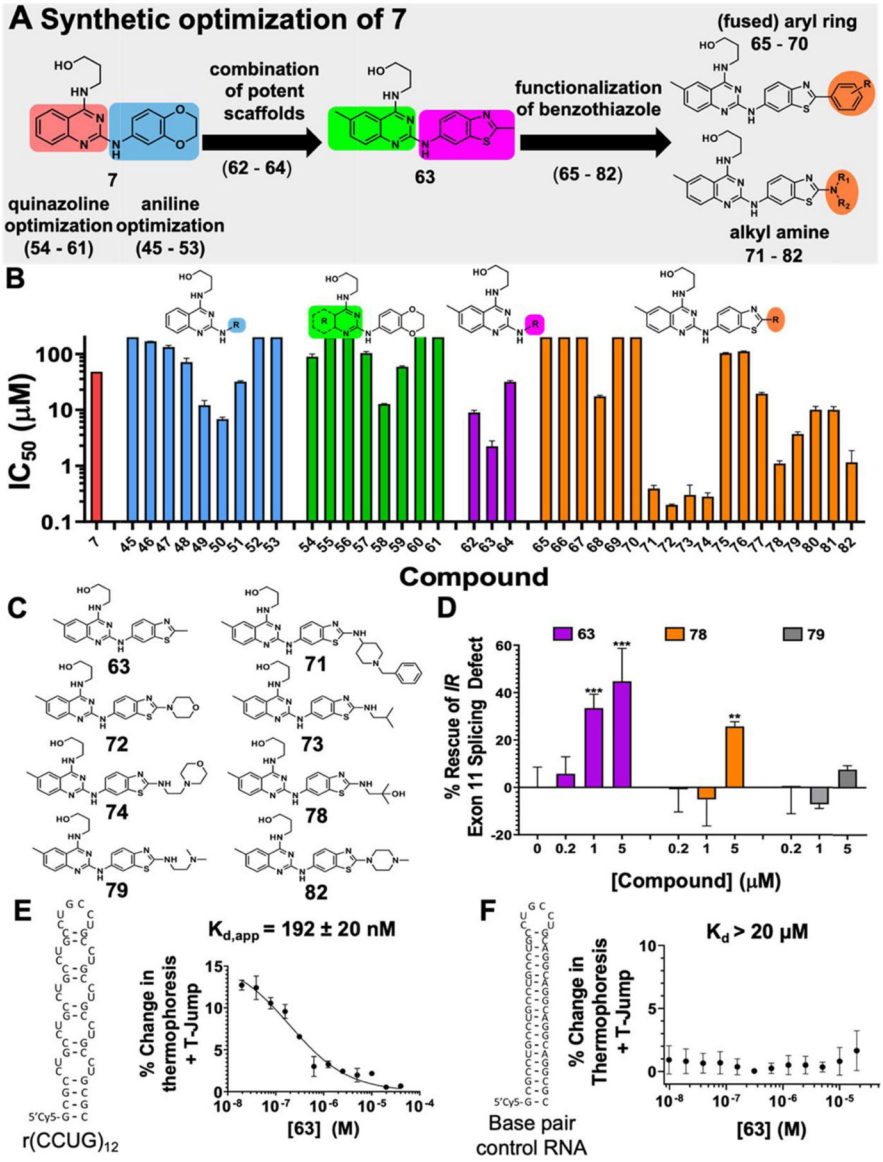

Figure 3.

Lead optimization of **7** and activity of analogues *in vitro* and in DM2 patient-derived fibroblasts. (A) Synthetic optimization scheme of compound **7**. (B) Structures of derivatives of **7** where "R" indicates the position(s) that were varied. IC_{50} values for disrupting the $r(CCUG)_{12}$–MBNL1 complex for each derivative ($n = 3$). (C) Structures of compounds with IC_{50}s < 5 μM. (D) Rescue of *IR* exon 11 mis-splicing by nontoxic compounds **63**, **79**, and **80** in DM2 patient-derived fibroblasts ($n = 3$). ** $P < 0.01$, *** $P < 0.001$, as determined by a one-way analysis of variance (ANOVA) relative to untreated ("0"). (E) Binding affinity curve of **63** and $r(CCUG)_{12}$ ($K_d = 192 \pm 20$ nM). (F) Binding affinity curve of **63** and a base pair control RNA ($K_d > 20$ μM). Error bars represent standard deviation (SD) for all panels.

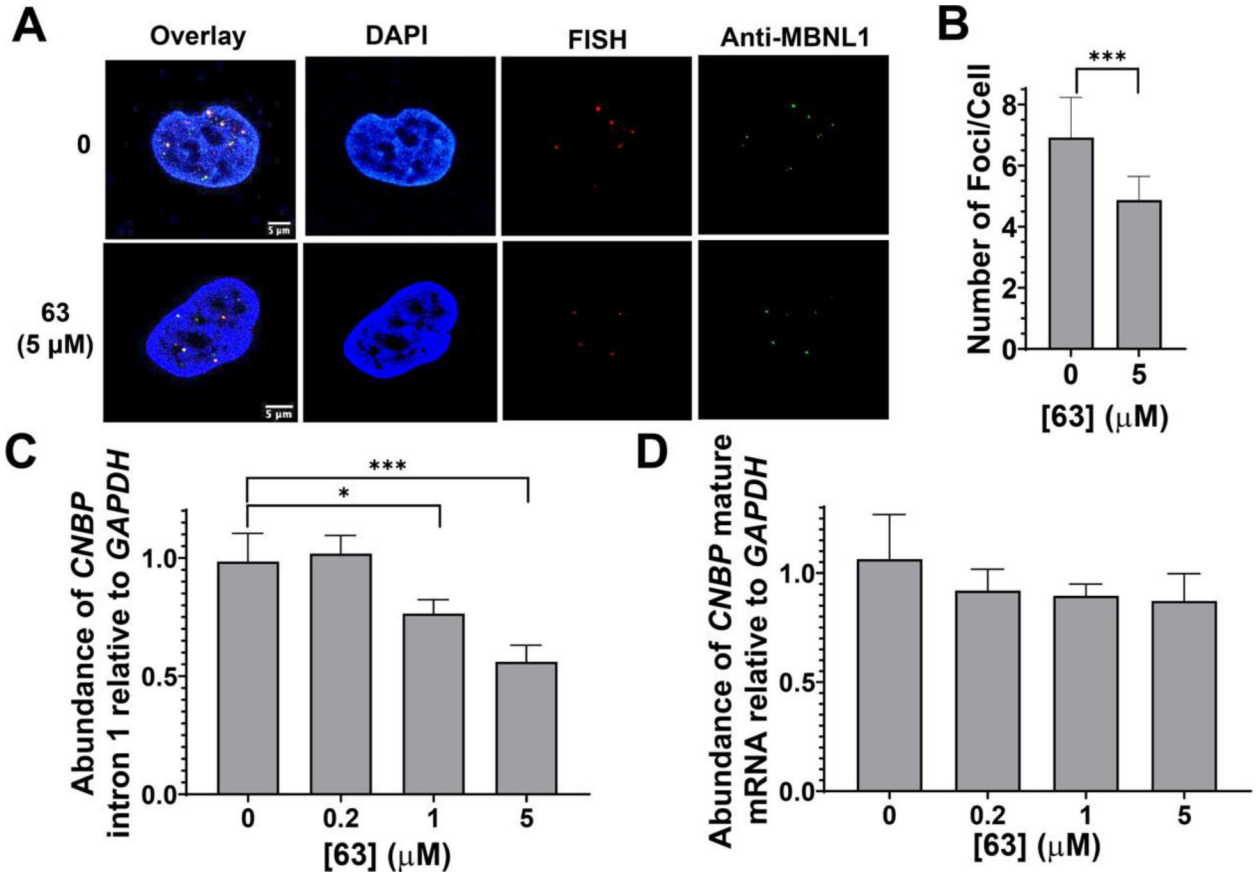

Figure 4.

Compound **63** rescues disease-associated defects in DM2 patient-derived fibroblasts. (A) Representative RNA FISH and MBNL1 immunofluorescence images of r(CCUG)^{exp}–MBNL1 foci. (B) Quantification of the number of nuclear foci/cell (n = 3, 40 nuclei counted/replicate). *** $P < 0.001$, as determined by a Student's t-test. (C) Analysis of CNBP intron 1 levels upon treatment with **63** via RT-qPCR (n = 3).* $P < 0.05$, *** $P < 0.001$, as determined by a one-way ANOVA. (D) Analysis of CNBP mature mRNA levels upon treatment with **63** via RT-qPCR (n = 3). Error bars represent standard deviation (SD) for all panels.